

Microscopic Derivation of the Ginzburg-Landau Equations for a d-wave Superconductor

D.L. Feder and C. Kallin

Department of Physics and Astronomy, McMaster University, Hamilton, Ontario L8S 4M1, Canada

(Received June 16, 2018)

The Ginzburg-Landau (GL) equations for a $d_{x^2-y^2}$ superconductor are derived within the context of two microscopic lattice models used to describe the cuprates: the extended Hubbard model and the Antiferromagnetic-van Hove model. Both models have pairing on nearest-neighbour links, consistent with theories for d-wave superconductivity mediated by spin fluctuations. Analytical results obtained for the extended Hubbard model at low electron densities and weak-coupling are compared to results reported previously for a d-wave superconductor in the continuum. The variation of the coefficients in the GL equations with carrier density, temperature, and coupling constants are calculated numerically for both models. The relative importance of anisotropic higher-order terms in the GL free energy is investigated, and the implications for experimental observations of the vortex lattice are considered.

74.20.-z, 74.20.De, 74.72.-h

I. INTRODUCTION

There is mounting experimental evidence to suggest that the high-temperature cuprate superconductors have an order parameter with unconventional symmetry.^{1,2} Indeed, recent Josephson interference measurements³ are strongly indicative of an order parameter with $d_{x^2-y^2}$ (d-wave) symmetry,⁴ which has line nodes along $|k_x| = |k_y|$. The linear density of states associated with the resulting low-energy excitations is thought⁵ to account for the linear temperature dependence of the specific heat⁶ as well as the linear temperature⁷ and magnetic field⁸ dependence of the penetration depth found for $\text{YBa}_2\text{Cu}_3\text{O}_{7-\delta}$ (123) and $\text{Bi}_2\text{Sr}_2\text{CaCu}_2\text{O}_y$ (2212).

A number of experimental results⁹ are consistent only with an order parameter of combined s-wave and d-wave symmetry. Sigrist and Rice¹⁰ have shown that in weakly orthorhombic cuprates (such as 2212 or 123) a small s-wave component would be present in addition to a critical d-wave order parameter. In tetragonal systems (such as the thallium compounds) that favour d-wave superconductivity, however, an s-wave component can only be nucleated locally near inhomogeneities¹¹ such as domain walls, impurities,¹² or vortices.¹³⁻¹⁶ Indeed, Soininen *et al.*¹³ investigated the structure of an isolated vortex for a d-wave superconductor within Bogoliubov-De Gennes theory and found that a non-zero s-wave component is induced in the vortex core. Their results, interpreted within the context of the relevant phenomenological Ginzburg-Landau (GL) free energy,¹⁷ imply a non-trivial topological structure for the additional s-wave component.¹⁴ As a consequence, the supercurrent and magnetic field distributions for an isolated vortex near H_{c1} exhibit a fourfold anisotropy in proportion to the magnitude of the s-wave component.¹⁶ In addition, the vortex-lattice structure near H_{c2} deviates significantly from the usual triangular Abrikosov lattice, becoming increasingly oblique with increasing s-wave admixture.^{14,16}

It remains uncertain, however, whether the anisotropy in the structures of an isolated vortex and the vortex lattice is indeed predominantly due to the admixture of an s-wave component. Ichioka *et al.*¹⁸ have shown that the inclusion of higher-order d-wave gradients in the GL free energy can give rise to a fourfold-symmetric current distribution around a vortex even in the absence of an induced s-wave component. One of the objectives of the present work is the clarification of this issue. Indeed, we find that the contributions to anisotropy of a fourth-order gradient term and the s-wave component are comparable, and tend to compete.

While phenomenological GL theory has been highly successful in predicting many interesting properties of d-wave superconductors in external fields, the relative magnitudes of the various coefficients appearing in the free energy and their dependence on temperature, filling, and field are presently unknown. An earlier derivation¹⁹ of the free energy from a continuum model could not include lattice effects that are believed to be important in theories of d-wave superconductivity. Consequently, as will be discussed later, certain technical difficulties arose which would not have appeared in the continuum limit of an appropriate lattice model. In any case, it would be useful to derive the GL free energy using models relevant to the high- T_c oxides. In the present work, the GL equations are derived microscopically within the context of two such models: the extended Hubbard and ‘Antiferromagnetic-van Hove’ models.

The extended Hubbard (EH) model, which includes a nearest-neighbour attraction in addition to the usual on-site repulsion, is one of the simplest lattice models which allows for a d-wave superconducting instability. Pairing

occurs along nearest-neighbour links, appropriate for theories where d-wave superconductivity is mediated by antiferromagnetic fluctuations (see Ref. 2 and references therein). It has been employed in several analytical²⁰ and numerical^{13,20,21} investigations of d-wave superconductivity. The EH model has recently been shown,²² however, to favour d-wave superconductivity only in a very small parameter space, preferring a phase separated or spin-density wave state.

The ‘Antiferromagnetic-van Hove’ (AvH) model²³ strongly favours d-wave superconductivity while incorporating the coexisting antiferromagnetic correlations observed in NMR,²⁴ neutron scattering,²⁵ and angle-resolved photoemission spectroscopy (ARPES)²⁶ experiments. High transition temperatures are obtained in the model due to the presence of a van Hove singularity in the hole density of states near the Fermi energy. An extended, flat band near $(\frac{\pi}{2}, \frac{\pi}{2})$ in momentum space is consistent with numerical investigations of a single hole propagating through an antiferromagnetic background²⁷, and with experimental evidence.²⁸ In the AvH model, holes are constrained to move within a single sublattice of a uniform antiferromagnetic background in order to minimize frustration. The hopping parameters are chosen to best fit the quasiparticle dispersion for YBCO measured using ARPES.²⁹

In Section II, the Ginzburg-Landau equations for the gap functions and supercurrent are derived microscopically for both the EH and AvH lattice models using a finite-temperature Green function method. The relations defining the transition temperatures are investigated in Section III. It is found that only a d-wave transition is favoured for the AvH model; the d-wave transition temperature $T_d \sim 100$ K is consistent with the high-temperature (high- T_c) oxides. The EH model, in contrast, can have either an s-wave or d-wave instability. S-wave is favoured at low electron densities while d-wave is favoured either at high densities or at lower densities with strong on-site repulsion. The equations for T_s (the s-wave transition temperature) and T_d are found analytically in the limit of weak-coupling and low electron densities. The corresponding analytical solutions for the AvH model are difficult to obtain due to the complicated angular dependence of the AvH dispersion. The GL free energy is derived for both models in Section IV. The coefficients of the GL equations are found analytically for the EH model in the same limit described above. The coefficients are calculated numerically for the EH model and for the AvH model near optimal doping. In section V, we summarize our results and discuss the experimental implications of the GL equations we have derived.

II. THE LATTICE GL EQUATIONS

The Hamiltonians for the extended Hubbard (EH) and antiferromagnetic-van Hove (AvH) models are respectively:

$$H^{\text{EH}} = -t \sum_{\langle ij \rangle \sigma} c_{i\sigma}^\dagger c_{j\sigma} e^{i \frac{2\pi}{\phi_0} \int_j^i \mathbf{A} \cdot d\mathbf{l}} - \mu \sum_{i\sigma} n_{i\sigma} + V_0 \sum_i n_{i\uparrow} n_{i\downarrow} - \frac{1}{2} \sum_{\langle ij \rangle \sigma\sigma'} V_{ij} n_{i\sigma} n_{j\sigma'}; \quad (2.1)$$

$$H^{\text{AvH}} = t_{11} \sum_{\langle\langle ij \rangle\rangle \sigma} c_{i\sigma}^\dagger c_{j\sigma} e^{i \frac{2\pi}{\phi_0} \int_j^i \mathbf{A} \cdot d\mathbf{l}} + t_{20} \sum_{\langle\langle\langle ij \rangle\rangle\rangle \sigma} c_{i\sigma}^\dagger c_{j\sigma} e^{i \frac{2\pi}{\phi_0} \int_j^i \mathbf{A} \cdot d\mathbf{l}} - \mu \sum_{i\sigma} n_{i\sigma} - \frac{V}{2} \sum_{\langle ij \rangle \sigma\sigma'} n_{i\sigma} n_{j\sigma'}, \quad (2.2)$$

where $n_{i\sigma} = c_{i\sigma}^\dagger c_{i\sigma}$, \mathbf{A} is the vector potential associated with the external magnetic field, $\phi_0 = hc/e$ is the flux quantum, and μ is the chemical potential included to fix the density. In the EH model the carriers are electrons, and positive V_0 and V_{ij} imply on-site repulsion and nearest-neighbour attraction, respectively. The superconducting carriers in the AvH model are holes propagating through the antiferromagnetic background of the undoped ‘parent’ state. Second and third nearest-neighbour hopping parameters are respectively $t_{11} = 0.04125$ eV and $t_{20} = 0.02175$ eV.²³ The absence of nearest-neighbour hopping in the AvH model reflects the restricted Hilbert space of the carriers; holes are constrained to move within a single spin sublattice in order to minimize frustration and preserve antiferromagnetic correlations. The values of t_{11} and t_{20} are chosen to result in a large density of states near the bottom of the hole band, located at $(\pi/2, \pi/2)$ in momentum space. The coefficient of the nearest-neighbour attraction $V = 0.075$ eV is chosen to yield a d-wave transition temperature $T_d \sim 100$ K at optimal doping ($\mu \approx -0.075$ eV, or hole density $\langle n \rangle \sim 0.2$), consistent with the high- T_c oxides.²³

If the lattice sites i and j are nearest-neighbours, we can write the mean-field EH Hamiltonian

$$H_{\text{eff}}^{\text{EH}}(B) = -t \sum_{\mathbf{r}, \vec{\delta}, \sigma} c_\sigma^\dagger(\mathbf{r} + \vec{\delta}) c_\sigma(\mathbf{r}) e^{i\phi_\delta} - \mu \sum_{\mathbf{r}, \sigma} c_\sigma^\dagger(\mathbf{r}) c_\sigma(\mathbf{r}) + \sum_{\mathbf{r}} [\Delta_\phi^*(\mathbf{r}) c_\downarrow(\mathbf{r}) c_\uparrow(\mathbf{r}) + H.c.] - \frac{1}{2} \sum_{\mathbf{r}, \vec{\delta}} [\Delta_\delta^*(\mathbf{r}) c_\downarrow(\mathbf{r}) c_\uparrow(\mathbf{r} + \vec{\delta}) - \Delta_\delta^*(\mathbf{r}) c_\uparrow(\mathbf{r}) c_\downarrow(\mathbf{r} + \vec{\delta}) + H.c.], \quad (2.3)$$

where

$$\phi_\delta = \frac{2\pi}{\phi_0} \int_{\mathbf{r}}^{\mathbf{r} + \vec{\delta}} \mathbf{A} \cdot d\mathbf{l}, \quad (2.4)$$

and $\vec{\delta} = \pm\hat{x}, \pm\hat{y}$ (the lattice constant is taken to be unity for convenience). The ‘on-site’ and nearest-neighbour gap functions are defined as follows:

$$\Delta_o(\mathbf{r}) \equiv V_0 \langle c_\downarrow(\mathbf{r}) c_\uparrow(\mathbf{r}) \rangle; \quad (2.5)$$

$$\begin{aligned} \Delta_\delta(\mathbf{r}) &\equiv V_\delta \langle c_\downarrow(\mathbf{r}) c_\uparrow(\mathbf{r} + \vec{\delta}) \rangle \\ &\equiv -V_\delta \langle c_\uparrow(\mathbf{r}) c_\downarrow(\mathbf{r} + \vec{\delta}) \rangle, \end{aligned} \quad (2.6)$$

assuming the existence of pairing in only the spin-singlet channel, in accordance with experimental results for the cuprate superconductors.³⁰ The mean-field Hamiltonian for the AvH model is written:

$$\begin{aligned} H_{\text{eff}}^{\text{AvH}}(B) &= t_{11} \sum_{\mathbf{r}, \vec{\delta}_{11}, \sigma} c_\sigma^\dagger(\mathbf{r} + \vec{\delta}_{11}) c_\sigma(\mathbf{r}) e^{i\phi_{\vec{\delta}_{11}}} + t_{20} \sum_{\mathbf{r}, \vec{\delta}_{20}, \sigma} c_\sigma^\dagger(\mathbf{r} + \vec{\delta}_{20}) c_\sigma(\mathbf{r}) e^{i\phi_{\vec{\delta}_{20}}} - \mu \sum_{\mathbf{r}, \sigma} c_\sigma^\dagger(\mathbf{r}) c_\sigma(\mathbf{r}) \\ &- \frac{1}{2} \sum_{\mathbf{r}, \vec{\delta}} [\Delta_\delta^*(\mathbf{r}) c_\downarrow(\mathbf{r}) c_\uparrow(\mathbf{r} + \vec{\delta}) + H.c.], \end{aligned} \quad (2.7)$$

where $\mathbf{r} = m\hat{r}_1 + n\hat{r}_2$, such that $\hat{r}_1 \equiv \hat{x} + \hat{y}$ and $\hat{r}_2 \equiv \hat{x} - \hat{y}$ are primitive vectors of a single sublattice, and each lattice site has the two-point basis $\hat{0}, \hat{x}$. Then, $\vec{\delta}_{11} = \pm\hat{r}_1, \pm\hat{r}_2$, $\vec{\delta}_{20} = \pm(\hat{r}_1 + \hat{r}_2), \pm(\hat{r}_1 - \hat{r}_2)$, and $\vec{\delta} = \pm\hat{x}, \pm\hat{y}$. Throughout the remainder of this section calculations will be presented within the context of the EH model. Comparison of the above Hamiltonians indicates that analogous results for the AvH model can be obtained at any stage by eliminating the on-site gap function, reversing the sign of the kinetic term (keeping in mind the holes hop along second and third-neighbour links), and setting $V_\delta = V/2$.

The Gor’kov equations can then be derived in the standard manner:³¹

$$\mathcal{G}(\mathbf{r}, \mathbf{r}', \omega_n) = \tilde{\mathcal{G}}^\circ(\mathbf{r}, \mathbf{r}', \omega_n) + \sum_{\mathbf{r}''} \tilde{\mathcal{G}}^\circ(\mathbf{r}, \mathbf{r}'', \omega_n) [\Delta_o(\mathbf{r}'') - \sum_{\vec{\delta}} \Delta_\delta(\mathbf{r}'') \hat{P}_\delta(\mathbf{r}'')] \mathcal{F}^\dagger(\mathbf{r}'', \mathbf{r}', \omega_n); \quad (2.8)$$

$$\mathcal{F}^\dagger(\mathbf{r}, \mathbf{r}', \omega_n) = - \sum_{\mathbf{r}''} \tilde{\mathcal{G}}^\circ(\mathbf{r}'', \mathbf{r}, -\omega_n) [\Delta_o^*(\mathbf{r}'') - \sum_{\vec{\delta}} \Delta_\delta^*(\mathbf{r}'') \hat{P}_\delta(\mathbf{r}'')] \mathcal{G}(\mathbf{r}'', \mathbf{r}', \omega_n), \quad (2.9)$$

where $\hat{P}_\delta(\mathbf{r}) X(\mathbf{r}) \equiv X(\mathbf{r} + \vec{\delta})$ is the kinetic energy operator, \mathcal{G} and \mathcal{F}^\dagger are finite-temperature single-particle and anomalous Green functions respectively, and $\tilde{\mathcal{G}}^\circ$ is the normal-state Green function in the presence of the external field. The Matsubara frequencies are $\omega_n \equiv \pi T(2n + 1)$. The anomalous Green function \mathcal{F}^\dagger is related to the gap functions:

$$\Delta_o^*(\mathbf{r}) = TV_0 \sum_{\omega_n} \mathcal{F}^\dagger(\mathbf{r}, \mathbf{r}, \omega_n), \quad (2.10)$$

$$\Delta_\delta^*(\mathbf{r}) = TV_\delta \sum_{\omega_n} \mathcal{F}^\dagger(\mathbf{r}, \mathbf{r} + \vec{\delta}, \omega_n), \quad (2.11)$$

Arbitrarily close to the superconducting critical temperature T_c , the ratios $\Delta_\alpha/T_c \ll 1$ or identically zero ($\vec{\alpha} = 0, \vec{\delta}$). Iterating Eqs. (2.8) and (2.9) up to third order in the gap functions, and making use of the conditions (2.10) and (2.11), the self-consistent equations for the gap functions are immediately obtained:

$$\begin{aligned} \frac{1}{V_\alpha} \Delta_\alpha^*(\mathbf{r}) &= - \sum_{\mathbf{r}'', \omega_n} \tilde{\mathcal{G}}^\circ(\mathbf{r}'', \mathbf{r}, -\omega_n) \Delta^*(\mathbf{r}'') \tilde{\mathcal{G}}^\circ(\mathbf{r}'', \mathbf{r} + \vec{\alpha}, \omega_n) \\ &+ \sum_{\mathbf{r}'', \mathbf{r}_1, \mathbf{r}_2, \omega_n} \tilde{\mathcal{G}}^\circ(\mathbf{r}'', \mathbf{r}, -\omega_n) \Delta^*(\mathbf{r}'') \tilde{\mathcal{G}}^\circ(\mathbf{r}'', \mathbf{r}_1, \omega_n) \Delta(\mathbf{r}_1) \tilde{\mathcal{G}}^\circ(\mathbf{r}_2, \mathbf{r}_1, -\omega_n) \Delta^*(\mathbf{r}_2) \tilde{\mathcal{G}}^\circ(\mathbf{r}_2, \mathbf{r} + \vec{\alpha}, \omega_n), \end{aligned} \quad (2.12)$$

where

$$\Delta^*(\mathbf{r}) \equiv \Delta_\circ^*(\mathbf{r}) - \sum_{\vec{\delta}} \Delta_\delta^*(\mathbf{r}) \hat{P}_\delta(\mathbf{r}), \quad (2.13)$$

and $\vec{\alpha} = \hat{0}, \pm \hat{x}$, or $\pm \hat{y}$.

In the strong type-II limit, appropriate for the high- T_c oxides, the penetration depth $\lambda(T)$ exceeds the coherence length $\xi(T)$ and all other length scales. The single-particle Green function is then approximately translationally invariant:

$$\begin{aligned} \tilde{\mathcal{G}}^\circ(\mathbf{r}, \mathbf{r}', \omega_n) &\approx \mathcal{G}^\circ(\mathbf{r} - \mathbf{r}', \omega_n) e^{-i\frac{2\pi}{\phi_0} \int_{\mathbf{r}}^{\mathbf{r}'} \mathbf{A} \cdot d\mathbf{l}} \\ &\approx \mathcal{G}^\circ(\mathbf{r} - \mathbf{r}', \omega_n) e^{i\frac{2\pi}{\phi_0} \mathbf{A}(\mathbf{r}) \cdot (\mathbf{r} - \mathbf{r}')}, \end{aligned} \quad (2.14)$$

where $\mathcal{G}^\circ(\mathbf{r} - \mathbf{r}', \omega_n)$ is the normal-state lattice Green function in the absence of an external field:

$$\mathcal{G}^\circ(\mathbf{r}, \omega_n) = \sum_{\mathbf{k}} \frac{e^{i\mathbf{k} \cdot \mathbf{x}}}{i\omega_n - \xi_k}, \quad (2.15)$$

and the sum is over wavevectors in the first Brillouin zone. The dispersion relations for the EH and AvH models are respectively

$$\xi_k^{\text{EH}} = -2t(\cos k_x + \cos k_y) - \mu \quad (2.16)$$

$$\xi_k^{\text{AvH}} = 2t_{11}(\cos k_1 + \cos k_2) + 4t_{20} \cos k_1 \cos k_2 - \mu, \quad (2.17)$$

where k_1 and k_2 are reciprocal vectors of a given sublattice. Assuming the gap functions vary slowly compared with the characteristic length scale k_F of the single-particle Green function (2.15), Eq. (2.12) can be expanded up to fourth-order in lattice derivatives. The justification for keeping higher-order gradient terms will be addressed in section V. The GL equations for the gap functions in the EH model can then be written:

$$\begin{aligned} \Delta_\alpha^*(\mathbf{r}) &= -TV_\alpha \sum_{\omega_n} \sum_{\vec{\alpha}'} (-1)^{\alpha'} \sum_{m,n} \mathcal{G}^\circ(m\hat{x} + n\hat{y}, -\omega_n) \mathcal{G}^\circ(m\hat{x} + n\hat{y} + \vec{\alpha}' - \vec{\alpha}, \omega_n) e^{-i\frac{2\pi}{\phi_0} \mathbf{A}(\mathbf{r}) \cdot (\vec{\alpha} - \vec{\alpha}')} \\ &\quad \left\{ 1 - \epsilon_{x,1}^{\text{EH}} (\hat{x}\Pi_x)^2 - \epsilon_{y,1}^{\text{EH}} (\hat{y}\Pi_y)^2 - \epsilon_{x,2}^{\text{EH}} (\hat{x}\Pi_x)^4 - \epsilon_{y,2}^{\text{EH}} (\hat{y}\Pi_y)^4 - \epsilon_{xy,2}^{\text{EH}} (\hat{x}\Pi_x)^2 (\hat{y}\Pi_y)^2 \right\} \Delta_{\alpha'}^*(\mathbf{r}) \\ &\quad + TV_\alpha \sum_{\mathbf{k}, \omega_n} \frac{e^{i\mathbf{k} \cdot \vec{\alpha}} e^{-i\frac{2\pi}{\phi_0} \mathbf{A}(\mathbf{r}) \cdot \vec{\alpha}}}{(\omega_n^2 + \xi_k^2)^2} \left\{ |\Delta_\circ(\mathbf{r})|^2 \Delta_\circ^*(\mathbf{r}) - 2|\Delta_\circ(\mathbf{r})|^2 M(\mathbf{r}) + 2|M(\mathbf{r})|^2 \Delta_\circ^*(\mathbf{r}) \right. \\ &\quad \left. - \Delta_\circ^2(\mathbf{r}) M^*(\mathbf{r}) + \Delta_\circ(\mathbf{r}) M^2(\mathbf{r}) - |M(\mathbf{r})|^2 M(\mathbf{r}) \right\}, \end{aligned} \quad (2.18)$$

where

$$i(\hat{z}\Pi_z) \Delta_{-z}(\mathbf{r}) \equiv e^{i\frac{4\pi}{\phi_0} A_z(\mathbf{r})} \Delta_z(\mathbf{r}) - \Delta_{-z}(\mathbf{r}) \quad (2.19)$$

$$\approx \left[(\hat{z}\hat{\Delta}_z) + i\frac{4\pi}{\phi_0} A_z(\mathbf{r}) \right] \Delta_{-z}(\mathbf{r}), \quad (2.20)$$

with the forward difference operator defined by

$$\begin{aligned} (\hat{z}\hat{\Delta}_z) \Delta_{-z}(\mathbf{r}) &\equiv \Delta_{-z}(\mathbf{r} + \hat{z}) - \Delta_{-z}(\mathbf{r}) \\ &= \Delta_z(\mathbf{r}) - \Delta_{-z}(\mathbf{r}), \end{aligned} \quad (2.21)$$

and

$$M(\mathbf{r}) \equiv \sum_{\vec{\delta}'=\pm\hat{x},\pm\hat{y}} \Delta_{\vec{\delta}'}^*(\mathbf{r}) e^{i\mathbf{k} \cdot \vec{\delta}'} e^{i\frac{2\pi}{\phi_0} \mathbf{A}(\mathbf{r}) \cdot \vec{\delta}'}. \quad (2.22)$$

The coefficients of the gradient terms have been defined in the Appendix for clarity. Note that all gap functions are taken at the same point \mathbf{r} in the last term of Eq. (2.18); this condition will be relaxed in Section V. The gradient

terms with odd powers of $\hat{x}\Pi_x$ and/or $\hat{y}\Pi_y$ vanish for tetragonal systems. The GL equations for the gap functions in the AvH model are given by:

$$\begin{aligned} \Delta_\delta^*(\mathbf{r}) &= \frac{TV}{2} \sum_{\omega_n} \sum_{\vec{\delta}'} \sum_{m,n} \mathcal{G}^\circ(m\hat{r}_1 + n\hat{r}_2, -\omega_n) \mathcal{G}^\circ(m\hat{r}_1 + n\hat{r}_2 + \vec{\delta}' - \vec{\delta}, \omega_n) e^{-i\frac{2\pi}{\phi_0} \mathbf{A}(\mathbf{r}) \cdot (\vec{\delta} - \vec{\delta}')} \\ &\quad \left\{ 1 - \epsilon_{x,1}^{\text{AvH}} (\hat{x}\Pi_x)^2 - \epsilon_{y,1}^{\text{AvH}} (\hat{y}\Pi_y)^2 - \epsilon_{x,2}^{\text{AvH}} (\hat{x}\Pi_x)^4 - \epsilon_{y,2}^{\text{AvH}} (\hat{y}\Pi_y)^4 - \epsilon_{xy,2}^{\text{AvH}} (\hat{x}\Pi_x)^2 (\hat{y}\Pi_y)^2 \right\} \Delta_{\vec{\delta}'}^*(\mathbf{r}) \\ &\quad - \frac{TV}{2} \sum_{\mathbf{k}, \omega_n} \frac{e^{i\mathbf{k} \cdot \vec{\delta}} e^{-i\frac{2\pi}{\phi_0} \mathbf{A}(\mathbf{r}) \cdot \vec{\delta}}}{(\omega_n^2 + \xi_k^2)^2} |M(\mathbf{r})|^2 M(\mathbf{r}), \end{aligned} \quad (2.23)$$

where we have used

$$(\hat{r}_1\Pi_{r1}) \equiv (\hat{x}\Pi_x) (\hat{y}\Pi_y) + (\hat{x}\Pi_x) + (\hat{y}\Pi_y); \quad (2.24)$$

$$(\hat{r}_2\Pi_{r2}) \equiv -(\hat{x}\Pi_x) (\hat{y}\Pi_y) + (\hat{x}\Pi_x) - (\hat{y}\Pi_y), \quad (2.25)$$

and the coefficients ϵ are given in the Appendix.

The current operator for the EH model is

$$\begin{aligned} \mathbf{j}^{\text{EH}}(\mathbf{r}) &= it \sum_{\vec{\delta}, \sigma} \vec{\delta} e^{i\phi_\delta} c_\sigma^\dagger(\mathbf{r} + \vec{\delta}) c_\sigma(\mathbf{r}) \\ &= -2tT \sum_{\vec{\delta}, \omega_n} \Pi'_\delta(\mathbf{r}') \mathcal{G}(\mathbf{r}, \mathbf{r}', \omega_n) \Big|_{\mathbf{r}=\mathbf{r}'} , \quad i\Pi'_\delta(\mathbf{r}) f(\mathbf{r}) \equiv e^{i\frac{2\pi}{\phi_0} \mathbf{A}(\mathbf{r}) \cdot \vec{\delta}} f(\mathbf{r} + \vec{\delta}) - f(\mathbf{r}) \end{aligned} \quad (2.26)$$

$$\rightarrow -2t \left[\vec{\Pi}'^*(\mathbf{r}) + \vec{\Pi}'(\mathbf{r}') \right] T \sum_{\omega_n} \mathcal{G}(\mathbf{r}, \mathbf{r}', \omega_n) \Big|_{\mathbf{r}=\mathbf{r}'} , \quad \vec{\Pi}'(\mathbf{r}) \equiv -i\vec{\nabla} + \frac{2\pi}{\phi_0} \mathbf{A}(\mathbf{r}), \quad (2.27)$$

where (2.27) represents the continuum limit of the lattice current. Iterating (2.8) and (2.9) to second order in gap functions and making the same approximations employed above, (2.26) becomes:

$$\begin{aligned} \mathbf{j}^{\text{EH}}(\mathbf{r}) &= 2tT \sum_{\substack{\vec{\delta}, \omega_n \\ \vec{\alpha}_1, \vec{\alpha}_2 \\ \mathbf{R}_1, \mathbf{R}_2}} e^{i\frac{2\pi}{\phi_0} \mathbf{A}(\mathbf{r}) \cdot (\vec{\alpha}_2 - \vec{\alpha}_1)} (-1)^{|\alpha_1|} (-1)^{|\alpha_2|} \mathcal{G}^\circ(-\mathbf{R}_1, \omega_n) \mathcal{G}^\circ(\mathbf{R}_2 - \mathbf{R}_1 - \vec{\alpha}_1, -\omega_n) \hat{\Delta}_{-\delta}(\mathbf{R}_2) \mathcal{G}^\circ(\mathbf{R}_2 + \vec{\alpha}_2, \omega_n) \\ &\quad \cdot \left\{ \Delta_{\alpha_2}^*(\mathbf{r}) [m(\hat{x}\Pi_x)^* + n(\hat{y}\Pi_y)^*] \Delta_{\alpha_1}(\mathbf{r}) + \Delta_{\alpha_1}(\mathbf{r}) [m'(\hat{x}\Pi_x) + n'(\hat{y}\Pi_y)] \Delta_{\alpha_2}^*(\mathbf{r}) \right\}, \end{aligned} \quad (2.28)$$

where $\mathbf{R}_1 = m\hat{x} + n\hat{y}$ and $\mathbf{R}_2 = m'\hat{x} + n'\hat{y}$. A similar expression for the AvH model can be obtained by setting $t \rightarrow -t_{11}, -t_{20}$ with $\vec{\delta} \rightarrow \vec{\delta}_{11}, \vec{\delta}_{20}$ and $\mathbf{R}_1 = m\hat{r}_1 + n\hat{r}_2$, $\mathbf{R}_2 = m'\hat{r}_1 + n'\hat{r}_2$, and making the replacements $(\hat{x}\Pi_x) \rightarrow (\hat{x}\Pi_x) + (\hat{y}\Pi_y)$ and $(\hat{y}\Pi_y) \rightarrow (\hat{x}\Pi_x) - (\hat{y}\Pi_y)$.

The various integrals and sums appearing in the Ginzburg-Landau equations for the gap functions (2.18), (2.23), and the current (2.28) can, in general, be determined only numerically. There is, however, one case which is analytically tractable: the EH model at low electron densities and weak to intermediate coupling. For $V_\delta = 0$ and $V_0 \rightarrow -V_0$, this limit would correspond to ordinary BCS theory.

III. DETERMINATION OF T_c

At temperatures sufficiently near T_c , we can linearize the gap equations (2.18) and (2.23). Making use of the definition of the normal-state Green function (2.15), we obtain for the EH model:

$$\Delta_\circ^*(\mathbf{r}) = TV_0 \sum_{\omega_n, \mathbf{k}} \frac{2a_k \Delta_s^*(\mathbf{r}) - \Delta_\circ^*(\mathbf{r})}{\omega_n^2 + \xi_k^2}, \quad (3.1)$$

$$\Delta_s^*(\mathbf{r}) = \frac{TV_1}{2} \sum_{\omega_n, \mathbf{k}} \frac{a_k [2a_k \Delta_s^*(\mathbf{r}) - \Delta_\circ^*(\mathbf{r})]}{\omega_n^2 + \xi_k^2}, \quad (3.2)$$

$$\Delta_d^*(\mathbf{r}) = TV_1 \sum_{\omega_n, \mathbf{k}} \frac{b_k^2 \Delta_d^*(\mathbf{r})}{\omega_n^2 + \xi_k^2}, \quad (3.3)$$

where $a_k = \cos k_x + \cos k_y$ and $b_k = \cos k_x - \cos k_y$. The s-wave and d-wave gap functions are related to the bond gap functions through the gauge-invariant definitions:³²

$$\Delta_s(\mathbf{r}) \equiv \frac{1}{4} \left[e^{-i\frac{2\pi}{\phi_0}A_x(\mathbf{r})} \Delta_x(\mathbf{r}) + e^{i\frac{2\pi}{\phi_0}A_x(\mathbf{r})} \Delta_{-x}(\mathbf{r}) + e^{-i\frac{2\pi}{\phi_0}A_y(\mathbf{r})} \Delta_y(\mathbf{r}) + e^{i\frac{2\pi}{\phi_0}A_y(\mathbf{r})} \Delta_{-y}(\mathbf{r}) \right], \quad (3.4)$$

$$\Delta_d(\mathbf{r}) \equiv \frac{1}{4} \left[e^{-i\frac{2\pi}{\phi_0}A_x(\mathbf{r})} \Delta_x(\mathbf{r}) + e^{i\frac{2\pi}{\phi_0}A_x(\mathbf{r})} \Delta_{-x}(\mathbf{r}) - e^{-i\frac{2\pi}{\phi_0}A_y(\mathbf{r})} \Delta_y(\mathbf{r}) - e^{i\frac{2\pi}{\phi_0}A_y(\mathbf{r})} \Delta_{-y}(\mathbf{r}) \right]. \quad (3.5)$$

(3.6)

The equations that determine the s-wave and d-wave transition temperatures T_s and T_d are immediately

$$[V_1 I_2(T_s) - 2] [V_0 I_0(T_s) + 2] = V_0 V_1 I_1^2(T_s); \quad (3.7)$$

$$I_3(T_d) = \frac{2}{V_1}, \quad (3.8)$$

where

$$I_n(T_s) \equiv \sum_{\mathbf{k}} \frac{a_k^n}{\xi_k} \tanh \left(\frac{\xi_k}{2T_s} \right), \quad n = 0, 1, 2; \quad (3.9)$$

$$I_3(T_d) \equiv \sum_{\mathbf{k}} \frac{b_k^2}{\xi_k} \tanh \left(\frac{\xi_k}{2T_d} \right). \quad (3.10)$$

It is clear from Eq. (3.7) that if $V_1 = 0$, no s-wave superconducting instability can occur for positive temperature.

The corresponding equations for the AvH model are

$$1 = \frac{V}{4} \sum_{\mathbf{k}} \frac{1 + \cos k_1 \cos k_2 + \cos k_1 + \cos k_2}{\xi_k} \tanh \left(\frac{\xi_k}{2T_s} \right), \quad (3.11)$$

$$1 = \frac{V}{4} \sum_{\mathbf{k}} \frac{1 + \cos k_1 \cos k_2 - \cos k_1 - \cos k_2}{\xi_k} \tanh \left(\frac{\xi_k}{2T_d} \right). \quad (3.12)$$

While these equations are not analytically tractable, they have been shown numerically²³ to strongly favour a d-wave transition temperature for all relevant hole concentrations. Optimal doping at approximately 25% filling (in the hole representation, where $\langle n_h \rangle$ is calculated at T_c) yields a value of $T_d \sim 100$ K.

In order to analytically solve the sums I_{1-4} , Eqs. (3.9) and (3.10), we make the standard transformation to an integration over energies, making use of the single-particle density of states (DOS)

$$N(\varepsilon) \equiv \sum_{\mathbf{k}} \delta(\varepsilon - \varepsilon_k) \approx \begin{cases} N(0) + N(1) \ln \left| \frac{D}{\varepsilon} \right|, & \text{if } |\varepsilon| \leq D; \\ 0, & \text{otherwise,} \end{cases} \quad (3.13)$$

where $D = 4t$ is the half-bandwidth and $\varepsilon_k \equiv \xi_k + \mu$. The DOS is approximated by a constant plus a term reflecting the van Hove singularity at half-filling ($\varepsilon = 0$), as is shown in Fig. 1. The best fit is obtained when $N(0) = 0.31/D$ (the DOS for free electrons in two dimensions is $1/\pi D$) and $N(1) = 0.19/D$ (note that the DOS at half-filling is approximately²⁰ $(2/\pi^2 D) \ln|D/\varepsilon|$). Using the relation $a_k = -2(\xi + \mu)/D$, the sums I_{0-2} can be solved to yield:

$$I_0(T_s) \approx 2N' \ln \left(\frac{T^*}{T_s} \right) - \frac{2D}{\mu} N(1); \quad (3.14)$$

$$I_1(T_s) \approx -\frac{4\mu}{D} N' \left[\ln \left(\frac{T^*}{T_s} \right) - 1 \right] + \frac{4\mu}{D} \left(1 + \frac{D}{\mu} \right) N(1); \quad (3.15)$$

$$I_2(T_s) \approx \frac{8\mu^2}{D^2} N' \ln \left(\frac{T^*}{T_s} \right) + \frac{4(D^2 - 3\mu^2)}{D^2} N(0) + \frac{2}{D^2} \left[-4\mu D + 6\mu^2 \ln \left| \frac{\mu}{D} \right| - 5\mu^2 + D^2 \right] N(1), \quad (3.16)$$

where

$$N' = N(0) - N(1) \ln \left| \frac{\mu}{D} \right|, \quad (3.17)$$

and

$$T^* \equiv \frac{2e^\gamma \sqrt{D^2 - \mu^2}}{\pi}. \quad (3.18)$$

For all terms proportional to $N(1)$, we assume that $T_c \ll D$ (weak-coupling), so that

$$\tanh \left(\frac{\varepsilon - \mu}{2T} \right) \approx \begin{cases} -1, \varepsilon < \mu; \\ +1, \varepsilon > \mu. \end{cases} \quad (3.19)$$

Note that in this lattice model, all interactions are instantaneous and therefore the bandwidth is the only possible energy cutoff. Since b_k cannot be written exactly in terms of ξ_k , some simplifying assumption must be made in order to evaluate I_3 . At low densities (the continuum limit of the lattice model), $\xi_k \approx tk^2 - D - \mu$ and thus $b_k \approx -2\cos 2\theta(\xi + D + \mu)/D$. Then,

$$\begin{aligned} I_3(T_d) &\approx \frac{4(\mu + D)^2}{D^2} N' \ln \left(\frac{T^*}{T_d} \right) + \frac{2}{D^2} (D^2 - 4\mu D - 3\mu^2) N(0) \\ &+ \frac{2}{D^2} \left[\frac{-2D}{\mu} (\mu + D)^2 + \mu(3\mu + 4D) \ln \left| \frac{\mu}{D} \right| + \frac{D^2 - 8\mu D - 5\mu^2}{2} \right] N(1). \end{aligned} \quad (3.20)$$

The equation for the s-wave transition temperature T_s resulting from the application of Eq. (3.7) is, for $V_0 = 0$:

$$T_s = T^* \exp \left\{ \frac{-D^2 - V_1 [6\mu^2 N' - 2D^2 N(0) - (D^2 - 4\mu D - 5\mu^2) N(1)]}{4\mu^2 V_1 N'} \right\}. \quad (3.21)$$

The corresponding equation for the d-wave transition temperature T_d from Eq. (3.8) is:

$$T_d = T^* \exp \left\{ \frac{-D^2 - V_1 [\mu(4D + 3\mu) N' - D^2 N(0) + \frac{1}{2\mu} (4D^3 + 7D^2\mu + 12D\mu^2 + 5\mu^3) N(1)]}{2(\mu + D)^2 V_1 N'} \right\}. \quad (3.22)$$

The transition temperatures for the cases $V_1 = t$ and $V_1 = 3t$ are shown as functions of chemical potential in Figs. 2 and 3 respectively. Near the bottom of the tight-binding band ($\mu \approx -D$), an s-wave transition is strongly favoured for any V_0 and V_1 , whereas a d-wave transition is favoured near half-filling ($\mu \approx 0$). The value of the chemical potential at which the preferred symmetry of the dominant gap function changes is extremely sensitive to the strengths of the respective interactions. As the on-site repulsion is increased, the magnitude of T_s is suppressed while T_d is unaffected.²⁰ As a result, d-wave superconductivity is favoured for virtually all densities for sufficiently large V_0 . It should be noted that the magnitude of the subcritical transition temperature, associated with the subdominant gap function, is in fact further decreased due to the presence of the dominant gap function. The relevant equation for the subcritical transition temperature, one of Eqs. (3.1)-(3.3), should have ξ_k replaced by $\sqrt{\xi_k^2 + \Delta_k^{\text{DOM}}}$, where Δ_k^{DOM} is the magnitude of the dominant gap function. Thus, the subcritical transition temperature, which is of dubious relevance in any case, can be taken to be identically zero without loss of generality.

IV. CALCULATION OF THE GINZBURG-LANDAU COEFFICIENTS

A. Extended Hubbard Model

For sufficiently large systems, the lattice sums in Eq. (2.18) can be transformed into k-space integrals. Neglecting fourth-order derivatives and making use of the expressions for the s-wave (3.4) and d-wave (3.5) gap functions as well as the normal-state Green function (2.15), the following three gap equations for the EH model are obtained:

$$\Delta_o^* = 4TV_0 \sum_{\omega_n} \int \frac{d^2k}{(2\pi)^2} \left\{ \frac{s^*(\mathbf{r}, \mathbf{k})}{\omega_n^2 + \xi_k^2} - \frac{1}{(\omega_n^2 + \xi_k^2)^2} \left[16|s(\mathbf{r}, \mathbf{k})|^2 s^*(\mathbf{r}, \mathbf{k}) + 32|d(\mathbf{r}, \mathbf{k})|^2 s^*(\mathbf{r}, \mathbf{k}) + 16d^{*2}(\mathbf{r}, \mathbf{k})s(\mathbf{r}, \mathbf{k}) \right] \right. \right. \\ \left. \left. - \int d^2z \frac{z^2}{2} \int \frac{d^2k'}{(2\pi)^2} \frac{e^{i(\mathbf{k}+\mathbf{k}')\cdot\mathbf{z}}}{(-i\omega_n - \xi_{k'})(i\omega_n - \xi_k)} (\cos^2\theta\Pi_x^2 + \sin^2\theta\Pi_y^2) [s^*(\mathbf{r}, \mathbf{k}) + d^*(\mathbf{r}, \mathbf{k})] \right\}; \quad (4.1)$$

$$\Delta_s^* = 2TV_1 \sum_{\omega_n} \int \frac{d^2k}{(2\pi)^2} a_k \left\{ \text{as above} \right\} \quad (4.2)$$

$$\Delta_d^* = 2TV_1 \sum_{\omega_n} \int \frac{d^2k}{(2\pi)^2} b_k \left\{ \frac{d^*(\mathbf{r}, \mathbf{k})}{\omega_n^2 + \xi_k^2} - \frac{1}{(\omega_n^2 + \xi_k^2)^2} \left[16|d(\mathbf{r}, \mathbf{k})|^2 d^*(\mathbf{r}, \mathbf{k}) + 32|s(\mathbf{r}, \mathbf{k})|^2 d^*(\mathbf{r}, \mathbf{k}) + 16s^{*2}(\mathbf{r}, \mathbf{k})d(\mathbf{r}, \mathbf{k}) \right] \right. \right. \\ \left. \left. - \int d^2z \frac{z^2}{2} \int \frac{d^2k'}{(2\pi)^2} \frac{e^{i(\mathbf{k}+\mathbf{k}')\cdot\mathbf{z}}}{(-i\omega_n - \xi_{k'})(i\omega_n - \xi_k)} (\cos^2\theta\Pi_x^2 + \sin^2\theta\Pi_y^2) [s^*(\mathbf{r}, \mathbf{k}) + d^*(\mathbf{r}, \mathbf{k})] \right\}, \quad (4.3)$$

where $s(\mathbf{r}, \mathbf{k}) \equiv \frac{a_k}{2} \Delta_s(\mathbf{r}) - \frac{1}{4} \Delta_o(\mathbf{r})$, $d(\mathbf{r}, \mathbf{k}) \equiv \frac{b_k}{2} \Delta_d(\mathbf{r})$, θ is the angle between \mathbf{r} and \mathbf{z} ($= m\hat{x} + n\hat{y}$), and the continuum limit of (2.19)

$$\Pi_z \equiv -i\frac{\partial}{\partial z} + \frac{4\pi}{\phi_0} A_z(\mathbf{r}) \quad (4.4)$$

acts only on the center of mass coordinate \mathbf{r} . Eqs. (4.1)-(4.3) can be simplified by making use of the fact that $\Delta_o(\mathbf{r}) = \epsilon \Delta_s(\mathbf{r})$, where ϵ depends on temperature and chemical potential. This relation follows from the observation that (4.1) and (4.2) are not linearly independent, since $\Delta_o(\mathbf{r})$ and $\Delta_s(\mathbf{r})$ have the same symmetry. Near T_c the magnitude of the s-wave component is small; from (3.1) we infer $\epsilon \approx V_0 I_1 / (1 + V_0 I_0/2)$, where I_0 and I_1 are defined in Eq. (3.9) and are evaluated in the weak-coupling and low-density limit in Eqs. (3.14) and (3.15). The integrals involving gradients of the gap functions can be greatly simplified by means of the identity:

$$\int d^2z x^2 G^o(\mathbf{z}, -\omega_n) G^o(\mathbf{z} + \vec{\alpha}, \omega_n) \equiv \int \frac{d^2k}{(2\pi)^2} e^{-i\mathbf{k}\cdot\vec{\alpha}} \left| \nabla_{k_x} G^o(\mathbf{k}, \omega_n) \right|^2, \quad (4.5)$$

and similarly for integrals involving y^2 . Thus,

$$\frac{1}{4} \left(1 - \frac{V_1 \epsilon^2}{4V_0} \right) \Delta_s^*(\mathbf{r}) = TV_1 \sum_{\omega_n} \int \frac{d^2k}{(2\pi)^2} \frac{a'_k}{\omega_n^2 + \xi_k^2} \left\{ a'_k \Delta_s^*(\mathbf{r}) \right. \\ \left. - \frac{1}{\omega_n^2 + \xi_k^2} \left[16a'_k{}^3 |\Delta_s(\mathbf{r})|^2 \Delta_s^*(\mathbf{r}) + 8a'_k b_k^2 |\Delta_d(\mathbf{r})|^2 \Delta_s^*(\mathbf{r}) + 4a'_k b_k^2 \Delta_d^{*2}(\mathbf{r}) \Delta_s(\mathbf{r}) \right. \right. \\ \left. \left. + \frac{D^2}{16} (\sin^2 k_x \Pi_x^2 + \sin^2 k_y \Pi_y^2) [2a'_k \Delta_s^*(\mathbf{r}) + b_k \Delta_d^*(\mathbf{r})] \right] \right\}, \quad (4.6)$$

$$\frac{1}{4} \Delta_d^*(\mathbf{r}) = TV_1 \sum_{\omega_n} \int \frac{d^2k}{(2\pi)^2} \frac{b_k}{\omega_n^2 + \xi_k^2} \left\{ \frac{1}{4} b_k \Delta_d^*(\mathbf{r}) \right. \\ \left. - \frac{1}{\omega_n^2 + \xi_k^2} \left[b_k^3 |\Delta_d(\mathbf{r})|^2 \Delta_d^*(\mathbf{r}) + 8a'_k{}^2 b_k |\Delta_s(\mathbf{r})|^2 \Delta_d^*(\mathbf{r}) + 4a'_k{}^2 b_k \Delta_s^{*2}(\mathbf{r}) \Delta_d(\mathbf{r}) \right. \right. \\ \left. \left. + \frac{D^2}{32} (\sin^2 k_x \Pi_x^2 + \sin^2 k_y \Pi_y^2) [2a'_k \Delta_s^*(\mathbf{r}) + b_k \Delta_d^*(\mathbf{r})] \right] \right\}, \quad (4.7)$$

where $a'_k \equiv \frac{a_k}{2} - \frac{\epsilon}{4}$.

The appropriate free energy for a d-wave (or extended s-wave) superconductor on a tetragonal lattice is:¹⁷

$$F_s = F_n + \alpha_s |\Delta_s(\mathbf{r})|^2 + \alpha_d |\Delta_d(\mathbf{r})|^2 + \beta_1 |\Delta_s(\mathbf{r})|^4 + \beta_2 |\Delta_d(\mathbf{r})|^4 \\ + \beta_3 |\Delta_s(\mathbf{r})|^2 |\Delta_d(\mathbf{r})|^2 + \beta_4 \left(\Delta_s^*(\mathbf{r})^2 \Delta_d^2(\mathbf{r}) + \Delta_d^*(\mathbf{r})^2 \Delta_s^2(\mathbf{r}) \right) \\ + \gamma_s |\vec{\Pi} \Delta_s(\mathbf{r})|^2 + \gamma_d |\vec{\Pi} \Delta_d(\mathbf{r})|^2 + \gamma_\nu \left[(\Pi_y \Delta_s(\mathbf{r}))^* (\Pi_y \Delta_d(\mathbf{r})) - (\Pi_x \Delta_s(\mathbf{r}))^* (\Pi_x \Delta_d(\mathbf{r})) + c.c. \right] \\ + F_1^s + F_1^d + \frac{h^2}{8\pi}, \quad (4.8)$$

where higher-order terms

$$F_1^s = \eta_s |\Delta_s(\mathbf{r}) \vec{\Pi} \Delta_s(\mathbf{r})|^2 + \gamma_{s+} |\vec{\Pi}^2 \Delta_s(\mathbf{r})|^2 + \gamma_{s-} |(\Pi_y^2 - \Pi_x^2) \Delta_s(\mathbf{r})|^2, \quad (4.9)$$

$$F_1^d = \eta_d |\Delta_d(\mathbf{r}) \vec{\Pi} \Delta_d(\mathbf{r})|^2 + \gamma_{d+} |\vec{\Pi}^2 \Delta_d(\mathbf{r})|^2 + \gamma_{d-} |(\Pi_y^2 - \Pi_x^2) \Delta_d(\mathbf{r})|^2 \quad (4.10)$$

will be discussed in detail in Section V. In the present work, the s-wave and d-wave order parameters are respectively the gap functions $\Delta_s(\mathbf{r})$ and $\Delta_d(\mathbf{r})$. The GL free energy (4.8) implies an s-wave (d-wave) component is induced whenever there exist spatial variations of the dominant d-wave (s-wave) order parameter. The magnitude of the ‘subdominant’ order parameter is evidently proportional to the coefficient γ_ν of the mixed gradient term. Minimizing and comparing to Eqs. (4.6) and (4.7) immediately yields:

$$\alpha_s = \frac{1}{V_1} - \frac{\epsilon^2}{4V_0} - 4T \sum_{\omega_n} \int \frac{d^2 k}{(2\pi)^2} \frac{a'_k{}^2}{\omega_n^2 + \xi_k^2} \quad ; \quad \alpha_d = \frac{1}{V_1} - T \sum_{\omega_n} \int \frac{d^2 k}{(2\pi)^2} \frac{b_k^2}{\omega_n^2 + \xi_k^2}, \quad (4.11)$$

$$\{\beta_1, \beta_2, \beta_3, \beta_4\} = T \sum_{\omega_n} \int \frac{d^2 k}{(2\pi)^2} \frac{\{32a'_k{}^4, 2b_k^4, 32a'_k{}^2 b_k^2, 8a'_k{}^2 b_k^2\}}{(\omega_n^2 + \xi_k^2)^2}, \quad (4.12)$$

$$\{\gamma_s, \gamma_\nu, \gamma_d\} = \frac{D^2}{8} T \sum_{\omega_n} \int \frac{d^2 k}{(2\pi)^2} \sin^2 k_x \frac{\{4a'_k{}^2, -2a'_k b_k, b_k^2\}}{(\omega_n^2 + \xi_k^2)^2}. \quad (4.13)$$

The current density in the xy plane can be obtained either by evaluating (2.28) in the continuum limit or by minimizing the free energy (4.8) with respect to the vector potential:

$$\begin{aligned} \mathbf{j} = \delta \frac{4\pi c}{\phi_0} & \left[\gamma_d \Delta_d^*(\mathbf{r}) \vec{\Pi} \Delta_d(\mathbf{r}) + \gamma_s \Delta_s^*(\mathbf{r}) \vec{\Pi} \Delta_s(\mathbf{r}) - \hat{x} \gamma_\nu \left(\Delta_s^*(\mathbf{r}) \Pi_x \Delta_d(\mathbf{r}) + \Delta_d^*(\mathbf{r}) \Pi_x \Delta_s(\mathbf{r}) \right) \right. \\ & \left. + \hat{y} \gamma_\nu \left(\Delta_s^*(\mathbf{r}) \Pi_y \Delta_d(\mathbf{r}) + \Delta_d^*(\mathbf{r}) \Pi_y \Delta_s(\mathbf{r}) \right) + c.c. \right], \end{aligned} \quad (4.14)$$

where the factor δ = (layer thickness/layer spacing) is introduced in order to model the layered structure of the cuprate superconductors. In the present two-dimensional model, $\delta \rightarrow 0$, reflecting the inability of the system to sustain screening currents. Eqs. (4.11)-(4.14) are subject to the following boundary conditions:

$$\mathbf{n} \cdot [\gamma_d \vec{\Pi} \Delta_d(\mathbf{r}) + \gamma_\nu (\hat{y} \Pi_y - \hat{x} \Pi_x) \Delta_s(\mathbf{r})] = 0, \quad (4.15)$$

$$\mathbf{n} \cdot [\gamma_s \vec{\Pi} \Delta_s(\mathbf{r}) + \gamma_\nu (\hat{y} \Pi_y - \hat{x} \Pi_x) \Delta_d(\mathbf{r})] = 0, \quad (4.16)$$

where \mathbf{n} is the unit vector normal to the surface of the superconductor.

The coefficients of the GL free energy can be calculated analytically in the same low-density and weak-coupling limit employed earlier by setting $a_k \approx -2\mu/D$, $b_k \approx -2(\mu + D)\cos 2\theta/D$ and $\sin^2 k_x \approx 4(\mu + D)\cos^2 \theta/D$. Making use of

$$T \sum_{\omega_n} \int \frac{d^2 k}{(2\pi)^2} \frac{1}{(\omega_n^2 + \xi_k^2)^2} \approx \frac{7\zeta(3)N'}{8\pi^2 T^2}, \quad (4.17)$$

we immediately obtain:

$$\alpha_s = -\frac{1}{V_1} \left(\frac{\mu}{D} + \frac{\epsilon}{4} \right)^2 \left(1 - \frac{T}{T_s} \right) \quad ; \quad \alpha_d = -\frac{1}{V_1} \left(\frac{\mu + D}{D} \right)^2 \left(1 - \frac{T}{T_d} \right), \quad (4.18)$$

$$\{\beta_1, \beta_2, \beta_3, \beta_4\} = 4\gamma \left\{ \left(\frac{\mu}{D} + \frac{\epsilon}{4} \right)^4, \frac{3}{8} \left(\frac{\mu + D}{D} \right)^4, 2 \left(\frac{\mu}{D} + \frac{\epsilon}{4} \right)^2 \left(\frac{\mu + D}{D} \right)^2, \frac{1}{2} \left(\frac{\mu}{D} + \frac{\epsilon}{4} \right)^2 \left(\frac{\mu + D}{D} \right)^2 \right\}, \quad (4.19)$$

$$\{\gamma_s, \gamma_\nu, \gamma_d\} = \gamma \frac{v_F^2}{16} \left\{ 2 \left(\frac{\mu}{D} + \frac{\epsilon}{4} \right)^2, - \left(\frac{\mu}{D} + \frac{\epsilon}{4} \right) \left(\frac{\mu+D}{D} \right), \left(\frac{\mu+D}{D} \right)^2 \right\} \quad (4.20)$$

where

$$\gamma = \frac{7\zeta(3)N'}{\pi^2 T^2}, \quad (4.21)$$

and $v_F^2 = D^2 k_F^2 / 4 \approx D(\mu + D)$. From (3.14) and (3.15) we obtain:

$$\epsilon = -\frac{4\mu}{D} \frac{V_0 N' \ln \left(\frac{T^*}{T} \right) - V_0 N'}{V_0 N' \ln \left(\frac{T^*}{T} \right) + 1}. \quad (4.22)$$

The expressions for α_s and α_d are only valid near their respective critical temperatures. Since the subcritical transition temperature is much lower than the dominant transition temperature, the corresponding coefficient for the subdominant order parameter can be assumed approximately $1/V_1$ for all values of $T < T_c$ (i.e. the contribution of the appropriate integral in either of (4.11) will be negligible). Note that in the limit $V_1 = 0$, $V_0 \rightarrow -V_0$, Δ_s and Δ_d vanish; the relevant gap equation is therefore Eq. (4.1) with $s(\mathbf{r}, \mathbf{k}) = \Delta_0(\mathbf{r})$ and $d(\mathbf{r}, \mathbf{k}) = 0$. Then Eq. (4.8) becomes the two-dimensional continuum BCS GL free energy:

$$F_s^{\text{BCS}} = F_n - \frac{1}{V_0} \left(1 - \frac{T}{T_s} \right) |\Delta_o(\mathbf{r})|^2 + \frac{7\zeta(3)N(0)}{16\pi^2 T^2} |\Delta_o(\mathbf{r})|^4 + \frac{7\zeta(3)N(0)}{32\pi^2 T^2} v_F^2 |\vec{\Pi} \Delta_o(\mathbf{r})|^2 + \frac{h^2}{8\pi}. \quad (4.23)$$

The GL coefficients (4.18)-(4.20) of the free energy (4.8) imply that at the bottom of the band ($\mu = -D$) the d-wave component vanishes, yielding a pure s-wave superconductor, while at half-filling ($\mu = 0$) only the d-wave component remains (with the caveat that these analytical results become decreasingly valid near half-filling). At densities intermediate between these two extremes all the GL coefficients are non-zero, leading to coexisting d-wave and s-wave order parameters for any temperature $T < T_c$ and finite external magnetic field. For type-II superconductors described by (4.8) in fields just above H_{c1} , it has been found^{14,19,16} that the subdominant order parameter is nucleated in the vicinity of a magnetic vortex core whenever the coefficient of the mixed-gradient term γ_ν is non-zero. Moving in the $x = y$ direction from the center of the vortex, the induced subdominant order parameter reaches a maximum, then decreases algebraically; there exist extra nodes in the $x = 0$ or $y = 0$ directions. The maximum amplitude attained by the subdominant order parameter nucleated in the vortex core is given by:¹⁶

$$\frac{\Delta_s(\Delta_d)^{\text{max}}}{\Delta_d(\Delta_s)^{\text{bulk}}} \approx \frac{3}{16} \frac{\gamma_\nu}{\gamma_{d(s)}} \frac{|\alpha_{d(s)}|}{\alpha_{s(d)}} \approx \frac{3}{16} \left(1 - \frac{T}{T_{d(s)}} \right) \frac{\gamma_\nu}{\gamma_{d(s)}}, \quad T_{d(s)} > T_{s(d)}, \quad (4.24)$$

where Δ_s^{max} is the maximum value of the induced subdominant s-wave order parameter compared with the magnitude of the critical d-wave order parameter Δ_d^{bulk} far from the vortex core, and vice versa. The estimates (4.24) are reliable as long as $\Delta_s(\Delta_d)^{\text{max}} < \Delta_d(\Delta_s)^{\text{bulk}}/4$, which is always the case sufficiently near T_c : since $\Delta_d(\Delta_s)^{\text{bulk}} \sim \sqrt{1 - T/T_c}$, the above equations indicate that

$$\Delta_s(\Delta_d)^{\text{max}} \sim (1 - T/T_c)^{3/2}. \quad (4.25)$$

The subdominant order parameter must decay more rapidly near the transition temperature since it is induced through spatial variations of the critical order parameter.

From (4.20), we have:

$$\frac{\gamma_\nu}{\gamma_d} \approx \left| \frac{\mu + D\epsilon/4}{\mu + D} \right|, \quad T_d > T_s. \quad (4.26)$$

$$\frac{\gamma_\nu}{\gamma_s} \approx \frac{1}{2} \left| \frac{\mu + D}{\mu + D\epsilon/4} \right|, \quad T_s > T_d, \quad (4.27)$$

The gradient coefficient ratios (4.26) and (4.27), which govern the magnitude of the subdominant order, are compared with the appropriate numerical results in Fig. 4 for the special case $V_0 = 0$. The analytical results capture the essential physics in their regime of applicability, i.e. at low densities and weak to intermediate coupling (better quantitative agreement at intermediate coupling can be obtained by including in a_k , b_k , etc. terms higher order in ξ_k). Near half-filling (zero-filling), where d-wave (s-wave) superconductivity is most stable, γ_ν/γ_d (γ_ν/γ_s) grows with increased

coupling. As a result, a significant component of the subdominant order parameter would only exist for stronger coupling in these two density regimes. It should be kept in mind, however, that as the on-site repulsion V_0 (and therefore ϵ) increases from zero, the magnitude of the s-wave component is suppressed for all densities; a d-wave subcomponent would be thereby enhanced in a bulk s-wave superconductor. The magnitude of the subdominant order parameter can be significantly larger even for weak coupling at intermediate densities, however; not only is the gradient coefficient ratio enhanced, but also the ratio $|\alpha_{\text{dom}}|/|\alpha_{\text{sub}}|$ since $\alpha_{\text{sub}} \rightarrow 0$ as the subdominant superconducting instability is approached. (Fig. 5 in the following section provides further quantitative details).

There are in general two characteristic length scales ξ_s and ξ_d governing spatial variations of the s-wave and d-wave order parameters in the vicinity of a vortex core, respectively. Near T_c , however, the induced subdominant order parameter is negligible compared to the critical order parameter by (4.25). Keeping only terms in the free energy (4.8) involving the dominant order parameter, the superconducting coherence lengths $\xi(T)$ and penetration depths $\lambda(T)$ near T_c can be crudely estimated:

$$\xi_{s(d)}(T) = \sqrt{\frac{\gamma_{s(d)}}{|\alpha_{s(d)}|}} \quad (4.28)$$

$$\lambda_{s(d)}(T) = \sqrt{\frac{2\phi_0^2\beta_{1(2)}}{\delta(4\pi)^3\gamma_{s(d)}|\alpha_{s(d)}|}} \quad (4.29)$$

where the flux quantum $\phi_0 = hc/e$ and both lengths are given in units of the lattice constant a . Inserting the relevant analytical expressions from Eqs. (4.18)-(4.20), valid in the low-density, weak-intermediate coupling limit, we obtain:

$$\xi_s(T) \approx \left(\frac{v_F}{2\pi T}\right) \sqrt{\frac{7\zeta(3)V_1N'}{2(1-T/T_s)}} \quad ; \quad \xi_d(T) \approx \left(\frac{v_F}{2\pi T}\right) \sqrt{\frac{7\zeta(3)V_1N'}{4(1-T/T_d)}}, \quad (4.30)$$

$$\lambda_s(T) \approx \sqrt{\frac{\phi_0^2V_1}{\pi^3\delta v_F^2(1-T/T_s)}} \quad ; \quad \lambda_d(T) \approx \sqrt{\frac{3\phi_0^2V_1}{4\pi^3\delta v_F^2(1-T/T_d)}}. \quad (4.31)$$

Note that the penetration depths are effectively infinite for an isolated layer. The magnitudes of the coherence lengths can be estimated for parameters stabilizing either s-wave or d-wave superconductivity (depending on the magnitude of V_0). For example, with $\mu = -2.0t$, $T_c \sim 0.2t$ ($V_1 \sim 3t$), and $T = 0.9T_c$, we obtain $\xi_d \sim 6a$ and $\xi_s \sim 8a$ for d-wave and s-wave superconductors respectively. The coherence lengths tend to become progressively shorter with increased electron density (Fig. 6 in the next section gives further details).

It is useful to compare the GL free energy (4.8) with that derived by Ren *et al.*¹⁹ Defining $s \equiv -(\frac{\mu}{D} + \frac{\epsilon}{4})\Delta_s$ and $d \equiv \frac{\mu+D}{D}\Delta_d$ (we drop reference to the center of mass coordinate \mathbf{r} for convenience), we obtain:

$$\begin{aligned} F_s = F_n - \left(1 - \frac{T}{T_s}\right)|s|^2 - \left(1 - \frac{T}{T_d}\right)|d|^2 + 4\gamma\left\{|s|^4 + \frac{3}{8}|d|^4 + 2|s|^2|d|^2 + \frac{1}{2}(s^{*2}d^2 + d^{*2}s^2)\right\} \\ + \gamma\frac{v_F^2}{16}\left\{2|\vec{\Pi}s|^2 + |\vec{\Pi}d|^2 + \left[(\Pi_y s)^*(\Pi_y d) - (\Pi_x s)^*(\Pi_x d) + c.c.\right]\right\} + \frac{h^2}{8\pi}. \end{aligned} \quad (4.32)$$

While the various coefficients appearing in the above free energy appear to be similar to those found by Ren *et al.*, one important distinction must be emphasized. The above free energy (4.32) mixes a d-wave order parameter with an *extended* s-wave order parameter. The analytical results suggest that only near half-filling ($\mu \rightarrow 0$) does the contribution of Δ_s to s vanish. At these densities, however, the approximations employed in the microscopic calculation above are not strictly valid; indeed, the numerical results clearly indicate the existence of a non-vanishing s-wave component for $T < T_d$ even in the absence of an on-site interaction (see Fig. 4). For any other density (except $\mu \rightarrow -D$, where the d-wave component vanishes) at temperatures below T_c , both Δ_s and Δ_d will be non-zero in the vortex core since both are generated by the same nearest-neighbour pairing interaction V_1 . There is therefore no limit in which the present model reduces to that of Ren *et al.*, i.e. where an isotropic s-wave order parameter derived from a repulsive on-site interaction is alone nucleated by spatial variations of a dominant d-wave order parameter. The technical difficulty which necessitated the implementation of the Padé approximation in Ref. 19 was due to the indistinguishability of Δ_0 and Δ_s in the continuum. This problem can always be avoided by starting with a lattice model which gives rise to a d-wave order parameter, then taking the appropriate continuum limit.

B. Antiferromagnetic-van Hove Model

Neglecting fourth-order derivatives, the equations for the gap functions in the thermodynamic limit of the AvH model from Eq. (2.23) are:

$$\Delta_s^* = \frac{TV}{2} \sum_{\omega_n} \int \frac{d^2 k}{(2\pi)^2} \left\{ \frac{c_k \Delta_s^*(\mathbf{r})}{\omega_n^2 + \xi_k^2} - \frac{1}{4(\omega_n^2 + \xi_k^2)^2} \left[c_k^2 |\Delta_s(\mathbf{r})|^2 \Delta_s^*(\mathbf{r}) + 2c_k d_k |\Delta_d(\mathbf{r})|^2 \Delta_s^*(\mathbf{r}) + c_k d_k \Delta_d^{*2}(\mathbf{r}) \Delta_s(\mathbf{r}) \right] \right. \right. \\ \left. \left. - \int d^2 z \frac{z^2}{2} \int \frac{d^2 k'}{(2\pi)^2} \frac{e^{i(\mathbf{k}+\mathbf{k}') \cdot \mathbf{z}}}{(-i\omega_n - \xi_{k'})(i\omega_n - \xi_k)} \left[\vec{\Pi}^2 + \sin 2\theta (\Pi_x^2 - \Pi_y^2) \right] [c_k \Delta_s^*(\mathbf{r}) + e_k \Delta_d^*(\mathbf{r})] \right\}; \quad (4.33)$$

$$\Delta_d^* = \frac{TV}{2} \sum_{\omega_n} \int \frac{d^2 k}{(2\pi)^2} \left\{ \frac{d_k \Delta_d^*(\mathbf{r})}{\omega_n^2 + \xi_k^2} - \frac{1}{4(\omega_n^2 + \xi_k^2)^2} \left[d_k^2 |\Delta_d(\mathbf{r})|^2 \Delta_d^*(\mathbf{r}) + 2c_k d_k |\Delta_s(\mathbf{r})|^2 \Delta_d^*(\mathbf{r}) + c_k d_k \Delta_s^{*2}(\mathbf{r}) \Delta_d(\mathbf{r}) \right] \right. \right. \\ \left. \left. - \int d^2 z \frac{z^2}{2} \int \frac{d^2 k'}{(2\pi)^2} \frac{e^{i(\mathbf{k}+\mathbf{k}') \cdot \mathbf{z}}}{(-i\omega_n - \xi_{k'})(i\omega_n - \xi_k)} \left[\vec{\Pi}^2 + \sin 2\theta (\Pi_x^2 - \Pi_y^2) \right] [e_k \Delta_s^*(\mathbf{r}) + d_k \Delta_d^*(\mathbf{r})] \right\}, \quad (4.34)$$

such that

$$c_k = 1 + \cos k_1 \cos k_2 + \cos k_1 + \cos k_2; \quad (4.35)$$

$$d_k = 1 + \cos k_1 \cos k_2 - \cos k_1 - \cos k_2; \quad (4.36)$$

$$e_k = \sin k_1 \sin k_2. \quad (4.37)$$

From these, and making use of (4.5), we can immediately obtain the appropriate free energy (4.8) where

$$\{\alpha_s, \alpha_d\} = \frac{1}{V} - \frac{1}{4} \int \frac{d^2 k}{(2\pi)^2} \frac{\{c_k, d_k\}}{\xi_k} \tanh \left(\frac{\xi_k}{2T} \right), \quad (4.38)$$

$$\{\beta_1, \beta_2, \beta_3, \beta_4\} = \frac{T}{16} \sum_{\omega_n} \int \frac{d^2 k}{(2\pi)^2} \frac{\{c_k^2, d_k^2, 4c_k d_k, c_k d_k\}}{(\omega_n^2 + \xi_k^2)^2}, \quad (4.39)$$

$$\{\gamma_s, \gamma_d\} = T \sum_{\omega_n} \int \frac{d^2 k}{(2\pi)^2} \frac{\sin^2 k_1 (t_{11} + 2t_{20} \cos k_2)^2 + \sin^2 k_2 (t_{11} + 2t_{20} \cos k_1)^2}{(\omega_n^2 + \xi_k^2)^2} \{c_k, d_k\}, \quad (4.40)$$

$$\gamma_\nu = -2T \sum_{\omega_n} \int \frac{d^2 k}{(2\pi)^2} \frac{e_k^2 (t_{11} + 2t_{20} \cos k_1) (t_{11} + 2t_{20} \cos k_2)}{(\omega_n^2 + \xi_k^2)^2}. \quad (4.41)$$

Note that $\beta_3 = 4\beta_4$, as was found for the EH model (4.32) and in Ref. 19. This generic feature of the free energy (4.8) is a direct consequence of the symmetry between the s-wave and d-wave order parameters and the underlying bond (or directionally-dependent) gap functions from which they are derived. Due to the complicated angular dependence of the AvH dispersion (2.17), the above expressions above are not analytically tractable, however. At optimal hole doping ($\langle n_{\text{hole}} \rangle = 1 - \langle n_{\text{electron}} \rangle \sim 0.2$), the d-wave transition temperature found using Eq. (3.12) is ~ 100 K, and the coefficients of the GL free energy have been evaluated numerically:

$$F_s = F_n - 11.3 \left(1 - \frac{T}{T_d} \right) |\Delta_d|^2 + 10.8 |\Delta_s|^2 + 38.7 |\Delta_s|^4 + 5720 |\Delta_d|^4 + 603 \left[|\Delta_s|^2 |\Delta_d|^2 + \frac{1}{4} \left(\Delta_s^{*2} \Delta_d^2 + \Delta_d^{*2} \Delta_s^2 \right) \right] \\ + 2.69 |\vec{\Pi} \Delta_s|^2 + 7.38 |\vec{\Pi} \Delta_d|^2 + 1.50 \left[(\Pi_y \Delta_s)^* (\Pi_y \Delta_d) - (\Pi_x \Delta_s)^* (\Pi_x \Delta_d) + c.c. \right] + \frac{h^2}{8\pi}, \quad (4.42)$$

where the coefficients β, γ have been evaluated at T_d .

The maximum value of the s-wave component nucleated in the vortex core, calculated numerically using (4.24), (4.11), (4.13), (4.38), and (4.40), is shown as a function of hole density in Fig. 5. Evidently, in the AvH model the induced s-wave component can be at most 5% of the bulk d-wave value (corresponding to $\langle n_h \rangle \sim 25\%$ and $T \rightarrow 0$, where it is assumed that $\alpha_d(T) \propto (1 - T/T_d), \forall T$). This is in spite of a large temperature-independent gradient coefficient ratio ($\gamma_\nu/\gamma_d \sim 20\%$ near optimal doping) that is found to increase monotonically with doping up to the

largest densities studied. By contrast, with a suitable choice of parameters (low T, V_0 , large $\langle n_h \rangle, V_1$), the EH model can allow for $s_{\max}/d_{\text{bulk}} \sim 20 - 30\%$. As the on-site repulsion is increased, however, the induced s-wave component is suppressed. The reduction in the magnitude of the s-wave component in the ‘overdoped’ AvH model may be partly due to effective on-site repulsion, built into the Hamiltonian by constraining holes to move within a single spin sublattice of an antiferromagnetic background.

The GL d-wave coherence length $\xi(T)$, calculated numerically with the aid of (4.28), is shown as a function of hole concentration for $T = 0.9T_d$ in Fig. 6. As expected, $\xi(T)$ becomes shorter with decreasing $\langle n_h \rangle$. For hole densities up to 30% filling, the AvH model leads to $\xi \sim a/\sqrt{1 - T/T_d}$ where a is a lattice spacing, in agreement with experiments for the cuprates.³³ The EH model yields similar d-wave coherence lengths for $V_1 = 2t, 3t$. These short ξ_d strictly violate the initial GL condition that the gap functions be more slowly varying than the Fermi wavelength $k_F^{-1} \sim 1a - 2a$, the characteristic length scale of the fermionic excitations. The close agreement, however, between the results of integrating Eqs. (4.8) and (4.14)^{14,19,16} and numerical investigations of short- ξ_d superconductors within Bogoliubov-De Gennes theory¹³ indicates that the GL equations derived thus far capture at least some of the essential physics.

V. EXTENSION OF THE GL EQUATIONS

The current and magnetic field distribution around an isolated vortex of a d-wave superconductor is found to be fourfold symmetric whenever an s-wave component is induced in the vicinity of the vortex core.^{16,19} It has been recently shown, however, that a similar anisotropy results from the inclusion of higher-order d-wave gradient terms in the GL free energy (4.8) even in the absence of an s-wave component.¹⁸ The connection between these observations can be made apparent by integrating out of the free energy the degree of freedom associated with the subdominant order parameter. Given a bulk d-wave superconductor, for example, Eq. (4.8) can be minimized with respect to $\Delta_s^*(\mathbf{r})$, yielding to lowest order in $(1 - T/T_d)$

$$\Delta_s(\mathbf{r}) = -\frac{\gamma_\nu}{\alpha_s}(\Pi_y^2 - \Pi_x^2)\Delta_d(\mathbf{r}). \quad (5.1)$$

Note that since $\Delta_d(\mathbf{r})$ varies on the length scale ξ_d , we immediately obtain $\Delta_s \sim \gamma_\nu/\alpha_s \xi_d^2 \sim (1 - T/T_d)^{3/2}$ in agreement with (4.25). Upon substitution of (5.1) into (4.8), the leading correction due to the induced s-wave component will be of the form $-\frac{\gamma_\nu^2}{\alpha_s} |(\Pi_y^2 - \Pi_x^2)\Delta_d|^2$. The free energy for an inhomogeneous d-wave superconductor then becomes:

$$F_s = F_n + \alpha_d |\Delta_d(\mathbf{r})|^2 + \beta_2 |\Delta_d(\mathbf{r})|^4 + \gamma_d |\vec{\Pi}\Delta_d(\mathbf{r})|^2 + \eta_d |\Delta_d(\mathbf{r})\vec{\Pi}\Delta_d(\mathbf{r})|^2 + \gamma_{d+} |\vec{\Pi}^2\Delta_d(\mathbf{r})|^2 + \left[\gamma_{d-} - \frac{\gamma_\nu^2}{\alpha_s} \right] |(\Pi_y^2 - \Pi_x^2)\Delta_d(\mathbf{r})|^2 + \frac{h^2}{8\pi}, \quad (5.2)$$

which clearly indicates that the induced s-wave order parameter breaks rotational symmetry in precisely the same way as a fourth-order d-wave gradient term.

In order to assess the relative importance of the induced subcritical component in eliciting anisotropy, the coefficients of the higher-order terms included in (4.8), and $\gamma_{d(s)-}$ in particular, must be determined microscopically. The derivation of η_s and η_d appearing in (4.9) and (4.10) requires extending the second term on the right hand side of Eq. (2.12) to include gradients of the gap functions. Applying similar techniques to those described in previous sections, one obtains for the EH model:

$$\begin{aligned} \{\eta_s, \eta_d\}^{\text{EH}} &= -4T \sum_{\omega_n} \int \frac{d^2k}{(2\pi)^2} \frac{\xi_k^2 (\nabla_{k_x} \xi_k)^2}{(\omega_n^2 + \xi_k^2)^4} \{16a'_k{}^4, b_k^4\} \\ &\approx -\frac{31\zeta(5)N'v_F^2}{32\pi^4 T^4} \left\{ \left(\frac{\mu}{D} + \frac{\epsilon}{4} \right)^4, \frac{3}{8} \left(\frac{\mu+D}{D} \right)^4 \right\}, \end{aligned} \quad (5.3)$$

where the analytical solution is valid in the continuum limit, i.e. at low electron densities. For the AvH model,

$$\{\eta_s, \eta_d\}^{\text{AvH}} = -2T \sum_{\omega_n} \int \frac{d^2k}{(2\pi)^2} \frac{\xi_k^2 \left[(\nabla_{k_1} \xi_k)^2 + (\nabla_{k_2} \xi_k)^2 \right]}{(\omega_n^2 + \xi_k^2)^4} \{c_k^2, d_k^2\}. \quad (5.4)$$

The coefficients of the fourth-order gradient terms can be derived by evaluating in the thermodynamic limit terms in (2.18) and (2.23) hitherto ignored. After some manipulation, one obtains

$$\begin{aligned}\{\gamma_{s\pm}, \gamma_{d\pm}\}^{\text{EH}} &= -\frac{T}{48} \sum_{\omega_n} \int d^2z \int \frac{d^2k d^2k'}{(2\pi)^4} \frac{e^{i(\mathbf{k}+\mathbf{k}')\cdot\mathbf{z}}}{(-i\omega_n - \xi_{k'})(i\omega_n - \xi_k)} x^2 (x^2 \pm 3y^2) \left\{ 4a'_k{}^2, b_k^2 \right\}, \\ \{\gamma_{s\pm}, \gamma_{d\pm}\}^{\text{AvH}} &= -\frac{T}{48} \sum_{\omega_n} \int d^2z \int \frac{d^2k d^2k'}{(2\pi)^4} \dots (r_1 + r_2)^2 \left[(r_1 + r_2)^2 \pm 3(r_1 - r_2)^2 \right] \{c_k, d_k\},\end{aligned}\quad (5.5)$$

where the ellipsis represents the k -dependent part of the integrand. The fourth-order gradient terms can be evaluated analytically in the EH model for weak to intermediate coupling and low densities:

$$\{\gamma_{s+}, \gamma_{d+}, \gamma_{s-}, \gamma_{d-}\} \approx -\frac{31\zeta(5)N'}{256} \left(\frac{v_F}{\pi T} \right)^4 \left\{ \frac{3}{2} \left(\frac{\mu}{D} + \frac{\epsilon}{4} \right)^2, \frac{5}{8} \left(\frac{\mu+D}{D} \right)^2, 0, \frac{2}{8} \left(\frac{\mu+D}{D} \right)^2 \right\}. \quad (5.6)$$

The analytical results obtained for the EH model indicate that all the higher-order terms in the free energy (4.9) and (4.10) have a negative sign compared with the second-order terms. The overall sign of these higher-order terms is of no consequence, however, provided the order parameters are sufficiently small and slowly varying; while both conditions will be satisfied near T_c , we also find $\gamma_{s(d)+}/\gamma_{s(d)} \sim (v_F/\pi T)^2 \rightarrow 0$ as $\mu \rightarrow -D$. At low densities, the EH model predicts a vanishing γ_{s-} coefficient, in accordance with the expectation that the free energy of a continuum s-wave superconductor should have spherical symmetry. Furthermore, $\gamma_{d+}/\gamma_{d-} = 5/2$, as was found by Ichioka *et al.*¹⁸

The analytical results for the EH model cannot adequately determine whether anisotropy in the free energy is primarily due to the existence of the subdominant order parameter or fourth-order gradients, however. For a bulk s-wave superconductor, the induced d-wave order parameter clearly breaks circular symmetry since $\gamma_\nu \neq 0$ for $\mu > -D$ while $\gamma_{s-} = 0$. Yet stronger coupling or lattice effects could lead to a non-vanishing γ_{s-} which could compete with the γ_ν^2/α_d coefficient in the free energy (5.2). Assuming that $\alpha_s \approx 1/V_1$, we find for a bulk d-wave superconductor

$$\frac{\gamma_\nu^2}{\alpha_s \gamma_{d-}} \approx -\frac{196\zeta(3)^2 V_1 N(0)}{31\zeta(5)} \left(\frac{\mu}{D} + \frac{\epsilon}{4} \right)^2, \quad (5.7)$$

which is of order $-V_1/t$. This result indicates that the ‘subcritical’ coefficient γ_ν^2/α_s and the ‘asymmetric’ coefficient γ_{d-} give similar contributions to the anisotropy. It should be emphasized, however, that d-wave superconductivity is not favoured at densities for which these analytical results are strictly valid.

The ratios $\gamma_\nu^2/\alpha_{d(s)}\gamma_{s(d)-}$ have been calculated numerically for $T = T_c$ and are shown in Fig. 7; virtually indistinguishable results have been obtained for all temperatures $0.5T_c \leq T \leq T_c$ (not shown). The numerics make clear that the contribution to anisotropy of the subcritical coefficient is at most comparable to the asymmetric coefficient for most densities and coupling strengths. Furthermore, since both coefficients have the same sign, their contributions to the asymmetric gradient term in the free energy (5.2) are in fact competing. Only for densities very near the crossover from bulk s-wave to d-wave condensation (or vice versa) in the EH model, or for large hole densities in the AvH model, does the subcritical coefficient dominate; in this regime $\alpha \rightarrow 0$.

It is not presently clear if the overall sign of the anisotropic fourth-order gradient term in the free energy (5.2) has any physical significance. Previous microscopic investigations of the EH model within the context of Bogoliubov-De Gennes theory¹³ demonstrated marked anisotropy in the structure of the critical d-wave component near the core of an isolated vortex. Parameters chosen correspond to a substantial s-wave component nucleated near the vortex core, i.e. $\gamma_\nu^2/\alpha_s \gg \gamma_{d-}$, and therefore a large negative coefficient for the asymmetric gradient term. Recent work,³⁴ however, indicates that this anisotropy persists even for densities approaching half-filling, where γ_{d-} dominates and the overall sign of the gradient term is positive.

For completeness, the coefficients $\eta_{s(d)}$ and $\gamma_{s(d)+}$ have also been determined numerically for both the EH and AvH models. Both coefficients are always negative and in general it is found that for the EH model $\eta_{s(d)} \sim 10\gamma_{s(d)+} \sim 100|\gamma_{s(d)-}|$, and $\gamma_{s(d)+}$ is of the same order as $\gamma_{s(d)}$ at T_c . For the AvH model at optimal doping and T_c , we obtain:

$$\begin{aligned}F_s^{\text{AvH}} &= F_n - 11.3 \left(1 - \frac{T}{T_d} \right) |\Delta_d(\mathbf{r})|^2 + 5720 |\Delta_d(\mathbf{r})|^4 + 7.38 |\vec{\Pi} \Delta_d(\mathbf{r})|^2 \\ &\quad - 16300 |\Delta_d(\mathbf{r}) \vec{\Pi} \Delta_d(\mathbf{r})|^2 - 16.5 |\vec{\Pi}^2 \Delta_d(\mathbf{r})|^2 + 2.65 |(\Pi_y^2 - \Pi_x^2) \Delta_d(\mathbf{r})|^2 + \frac{h^2}{8\pi}.\end{aligned}\quad (5.8)$$

The relatively large values of $\eta_{s(d)}$ and $\gamma_{s(d)+}$ compared with the magnitude of $\gamma_{s(d)}$ clearly demonstrates that the GL theory derived herein is only strictly valid quite near T_c .

VI. SUMMARY AND DISCUSSION

The primary objective of the present work has been to derive the Ginzburg-Landau equations for a d-wave superconductor using two microscopic lattice models which have been previously used to describe the high- T_c oxides: the extended Hubbard model and the Antiferromagnetic-van Hove model. In so doing, it has been possible to quantitatively investigate how the lattice and external magnetic field generate, and govern the interplay between, co-existing s-wave and d-wave order parameters. In addition, the relative magnitudes of the various GL coefficients, as well as their temperature and density dependence, have been ascertained.

Phenomenological GL theory has enabled much progress to be made recently toward understanding the structures of isolated vortices and the vortex lattice for d-wave superconductors. Of particular current interest is the theoretical prediction by Franz *et al.*^{14,16} of an oblique structure for the vortex lattice near H_{c2} , i.e. the Abrikosov lattice would be intermediate between the usual triangle and a square. The degree of ‘obliqueness’ is mostly dependent on the gradient coefficient ratio γ_ν/γ_d . The coefficient γ_ν governs the extent an s-wave component is induced by spatial variations of the dominant d-wave order parameter, and characterizes the degree of fourfold symmetry in the free energy. For $\gamma_\nu/\gamma_d = 0$, the s-wave component vanishes, yielding a triangular lattice. The Abrikosov lattice deforms continuously away from a triangle as γ_ν/γ_d is increased; for $\gamma_\nu/\gamma_d = 0.45$, the angle between primitive vectors $\phi = 76^\circ$. For $\gamma_\nu/\gamma_d \sim 0.6$ and higher, the flux lattice is square.

The present work demonstrates that microscopic models used to describe the high- T_c oxides can predict a significant admixture of an s-wave order parameter in the mixed state of a d-wave superconductor. One consequence is the deviation of the flux lattice from that of a triangle. It has been found that within a broad and experimentally relevant parameter space both microscopic models yield a gradient coefficient ratio $\gamma_\nu/\gamma_d \sim 0.1 - 0.4$. This is consistent with two recent experimental observations^{35,36} for YBCO of flux lattices with $\phi \approx 73^\circ$ and 77° . It is not yet clear, however, whether the $a - b$ anisotropy associated with the orthorhombicity of YBCO is alone sufficient to account for the distortion in the flux lattice.³⁷

It is presently uncertain whether the s-wave component nucleated in the vicinity of vortex cores is in fact required to induce a significant deviation from a triangular vortex lattice. It has been shown that a fourth-order gradient term in the d-wave order parameter also introduces fourfold symmetry into the free energy; over much of the phase diagram, the contribution of this term to anisotropy is comparable to that of the s-wave component. This important issue will be addressed in future work.

Wherever possible, comparison has been made with previous derivations of the GL coefficients within continuum models. It should be emphasized, however, that lattice models not only provide considerably more information regarding the density and coupling-dependence of s-wave and d-wave admixture in the vortex core, but also avoid the technical difficulties (i.e. the application of the Padé approximation) encountered in continuum models. In particular, the lattice models clearly indicate that both s-wave and d-wave components must always coexist in the vortex core for all temperatures below T_c , regardless of the symmetry of the bulk order parameter.

ACKNOWLEDGMENTS

The authors are grateful to W. Atkinson, A.J. Berlinsky, M. Franz, A. Nazarenko, C. O’Donovan, M.I. Salkola, and P.I. Soininen for numerous helpful comments and suggestions. This work has been partially supported by the Natural Sciences and Engineering Research Council of Canada and by the Ontario Centre for Materials Research.

APPENDIX: COEFFICIENTS OF THE GL GRADIENT TERMS

The coefficients of the gradient terms appearing in the GL equations for the gap functions (2.18) and (2.23) are, for the EH model:

$$\epsilon_{x,1}^{\text{EH}} = \frac{1}{2}|m|(|m| - 1); \quad (\text{A1})$$

$$\epsilon_{y,1}^{\text{EH}} = \frac{1}{2}|n|(|n| - 1); \quad (\text{A2})$$

$$\epsilon_{x,2}^{\text{EH}} = -\frac{1}{24}|m|(|m| - 1)(|m| - 2)(|m| - 3); \quad (\text{A3})$$

$$\epsilon_{y,2}^{\text{EH}} = -\frac{1}{24}|n|(|n| - 1)(|n| - 2)(|n| - 3); \quad (\text{A4})$$

$$\epsilon_{xy,2}^{\text{EH}} = -\frac{1}{4}|m|(|m|-1)|n|(|n|-1). \quad (\text{A5})$$

For the AvH model, we obtain:

$$\epsilon_{x,1}^{\text{AvH}} = \frac{1}{2} \left[|m|(|m|-1) + |n|(|n|-1) + 2mn \right]; \quad (\text{A6})$$

$$\epsilon_{y,1}^{\text{AvH}} = \frac{1}{2} \left[|m|(|m|-1) + |n|(|n|-1) - 2mn \right]; \quad (\text{A7})$$

$$\begin{aligned} \epsilon_{x,2}^{\text{AvH}} = & -\frac{1}{24} \left[|m|(|m|-1)(|m|-2)(|m|-3) + |n|(|n|-1)(|n|-2)(|n|-3) \right] \\ & - \frac{1}{12} |m||n| \left\{ 3(|m|-1)(|n|-1) + 2 \left[(|m|-1)(|m|-2) + (|n|-1)(|n|-2) \right] \right\}; \end{aligned} \quad (\text{A8})$$

$$\begin{aligned} \epsilon_{y,2}^{\text{AvH}} = & -\frac{1}{24} \left[|m|(|m|-1)(|m|-2)(|m|-3) + |n|(|n|-1)(|n|-2)(|n|-3) \right] \\ & - \frac{1}{12} |m||n| \left\{ 3(|m|-1)(|n|-1) - 2 \left[(|m|-1)(|m|-2) + (|n|-1)(|n|-2) \right] \right\}; \end{aligned} \quad (\text{A9})$$

$$\epsilon_{xy,2}^{\text{AvH}} = -\frac{1}{4} \left[\left(|m|(|m|-1) + |n|(|n|-1) \right)^2 - 4m^2n^2 \right]. \quad (\text{A10})$$

¹ For reviews see E. Dagotto, Rev. Mod. Phys. **66**, 763 (1994); D.J. Van Harlingen, Rev. Mod. Phys. **67**, 515 (1995).

² D.J. Scalapino, Phys. Rep. **250**, 331 (1995).

³ D.A. Wollman, D.J. Van Harlingen, W.C. Lee, D.M. Ginsberg and A.J. Leggett, Phys. Rev. Lett. **71**, 2134 (1993); C.C. Tsuei, J.R. Kirtley, C.C. Chi, L.S. Yu-Jahnes, A. Gupta, T. Shaw, J.Z. Sun and M.B. Ketchen, Phys. Rev. Lett. **73**, 593 (1994); A. Mathai, Y. Gim, R.C. Black, A. Amar and F.C. Wellstood, Phys. Rev. Lett. **74**, 4523 (1995); C.C. Tsuei, *et al.* Science, **271**, 329 (1996).

⁴ M. Sigrist and T.M. Rice, Rev. Mod. Phys. **67**, 503 (1995).

⁵ J. Annett, *et al.*, Phys. Rev. B **43**, 2778 (1991); S.K. Yip and J.A. Sauls, Phys. Rev. Lett. **69**, 2264 (1992).

⁶ K.A. Moler, D.J. Baar, J.S. Urbach, R. Liang, W.N. Hardy and A. Kapitulnik, Phys. Rev. Lett. **73**, 2744 (1994).

⁷ W.N. Hardy, D.A. Bonn, D.C. Morgan, R. Liang and K. Zhang, Phys. Rev. Lett. **70**, 3999 (1993); J.E. Sonier *et al.*, Phys. Rev. Lett. **72**, 744 (1994).

⁸ A. Maeda, Y. Iino, T. Hanaguri, K. Kishio and T. Fukase, Phys. Rev. Lett. **74**, 1202 (1995).

⁹ J. Ma, C. Quitman, R.J. Kelley, H. Bergen, C. Margaritondo and M. Onellion, Science **267**, 862 (1995); H. Ding, J.C. Campuzano and G. Jennings, Phys. Rev. Lett. **74**, 2784 (1995); A.G. Sun, D.A. Gajewski, M.B. Maple and R.C. Dynes, Phys. Rev. Lett. **72**, 2267 (1994).

¹⁰ M. Sigrist and T.M. Rice, Z. Phys. B - Cond. Matt. **68**, 9 (1987).

¹¹ G.E. Volovik, JETP Lett. **58**, 469 (1993).

¹² M. Franz, C. Kallin and A.J. Berlinsky, preprint.

¹³ P.I. Soininen, C. Kallin and A.J. Berlinsky, Phys. Rev. B **50**, 13883 (1994).

¹⁴ A.J. Berlinsky, A.L. Fetter, M. Franz, C. Kallin and P.I. Soininen, Phys. Rev. Lett. **75**, 2200 (1995).

¹⁵ M. Ichioka, N. Enomoto, N. Hayashi and K. Machida, Phys. Rev. B **53**, 2233 (1996).

¹⁶ M. Franz, C. Kallin, P.I. Soininen, A.J. Berlinsky and A.L. Fetter, Phys. Rev. B **53**, 5795 (1996).

¹⁷ R. Joynt, Phys. Rev. B **41**, 4271 (1990).

¹⁸ M. Ichioka, N. Enomoto, N. Hayashi and K. Machida, preprint.

¹⁹ Y. Ren, J.-H. Xu and C.S. Ting, Phys. Rev. Lett. **74**, 3680 (1995); J.-H. Xu, Y. Ren and C.S. Ting, Phys. Rev. B **52**, 7663 (1995).

²⁰ R. Micnas, J. Ranninger, S. Robaszkiewicz and S. Tabor, Phys. Rev. B **37**, 9410 (1988); R. Micnas, J. Ranninger and S. Robaszkiewicz, Rev. Mod. Phys. **62**, 113 (1990).

²¹ Y. Wang and A.H. MacDonald, Phys. Rev. B **52**, R3876 (1995).

²² A. Nazarenko, A. Moreo, J. Riera and E. Dagotto, preprint, cond-mat/9509155.

²³ E. Dagotto, A. Nazarenko and A. Moreo, Phys. Rev. Lett. **74**, 310 (1995).

²⁴ T. Imai *et al.*, Phys. Rev. B **47**, 9158 (1993).

²⁵ G. Aepli, Proceedings of the Stanford Conference on "Spectroscopies in Novel Superconductors", March 1995.

²⁶ P. Aebi *et al.*, Phys. Rev. Lett. **72**, 2757 (1994).

²⁷ E. Dagotto, A. Nazarenko and M. Boninsegni, Phys. Rev. Lett. **73**, 728 (1994); N. Bulut, D.J. Scalapino and S.R. White, Phys. Rev. B **50**, 7215 (1994).

²⁸ D.S. Dessau *et al.*, Phys. Rev. Lett. **71**, 2781 (1993); K. Gofron *et al.*, J. Phys. Chem. Solids **54**, 1193 (1993).

²⁹ A.A. Abrikosov, J.C. Campuzano and K. Gofron, Physica (Amsterdam) **214C**, 73 (1993).

³⁰ C.P. Slichter, J. Phys. Chem. Solids, **54**, 1439 (1993).

³¹ L.P. Gor'kov, Soviet Phys. JETP **9**, 1364 (1959); L.P. Gor'kov, Soviet Phys. JETP **10**, 998 (1960).

³² The inversion of these equations requires the imposition of boundary conditions since the s-wave and d-wave gap functions on any given site are tied to those at adjacent sites. Periodic boundary conditions are assumed throughout the present work.

³³ G. Burns, *High-Temperature Superconductivity*, (Academic Press, 1992).

³⁴ M.I. Salkola, private communication.

³⁵ B. Keimer, J.W. Lynn, R.W. Erwin, F. Dogan, W.Y. Shih and I.A. Aksay, J. Appl. Phys. **76**, 1 (1994).

³⁶ I. Maggio-Aprile, C. Renner, A. Erb, E. Walker and Ø. Fisher, Phys. Rev. Lett. **75**, 2754 (1995).

³⁷ M.B. Walker and T. Timusk, Phys. Rev. B **52**, 97 (1995).

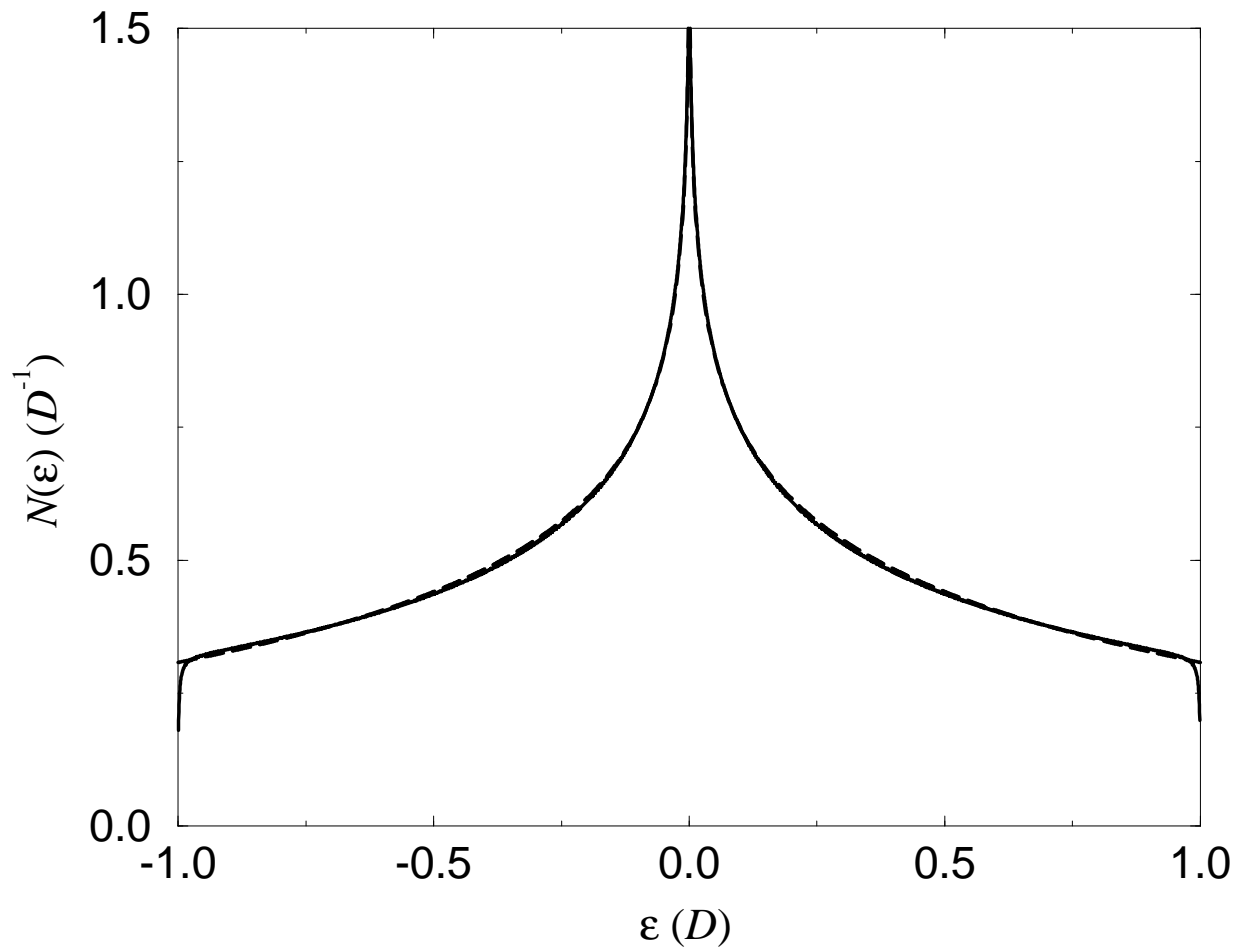


FIG. 1. The density of states $N(\varepsilon)$ for tight-binding electrons on the square lattice is shown as the solid curve. The energy scale is the half-bandwidth $D = 4t$. The best fit, the dashed line, is found to be $N(\varepsilon) = \frac{0.31}{D} + \frac{0.19}{D} \ln \left| \frac{D}{\varepsilon} \right|$.

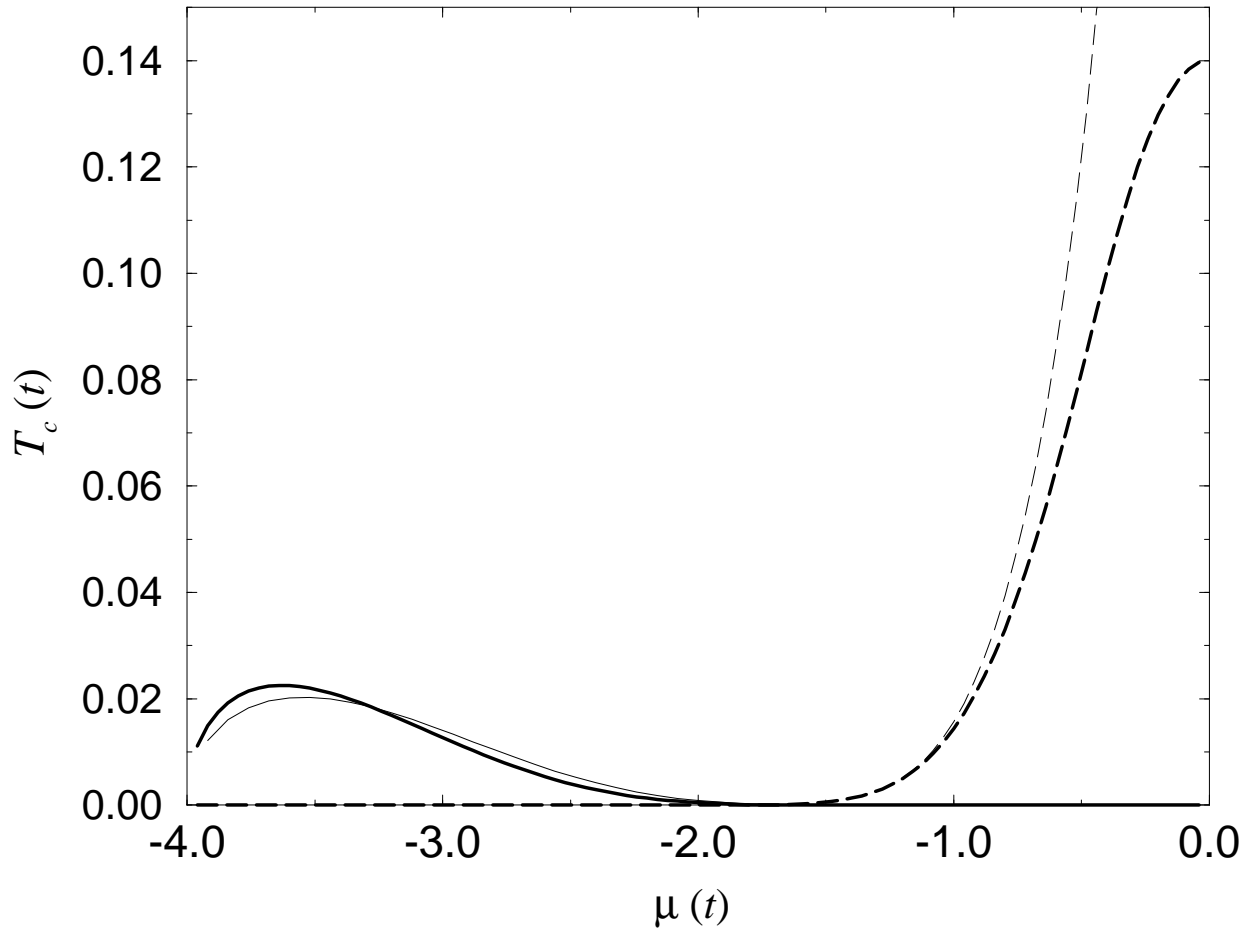


FIG. 2. The transition temperatures T_c are given as functions of chemical potential μ for nearest-neighbour attraction $V_1 = t$ and $V_0 = 0$. The results for T_s and T_d are given by solid and dashed lines, respectively. The analytical results (lighter lines) are found to compare well with the numerical results (darker lines) in the applicable low-density regime.

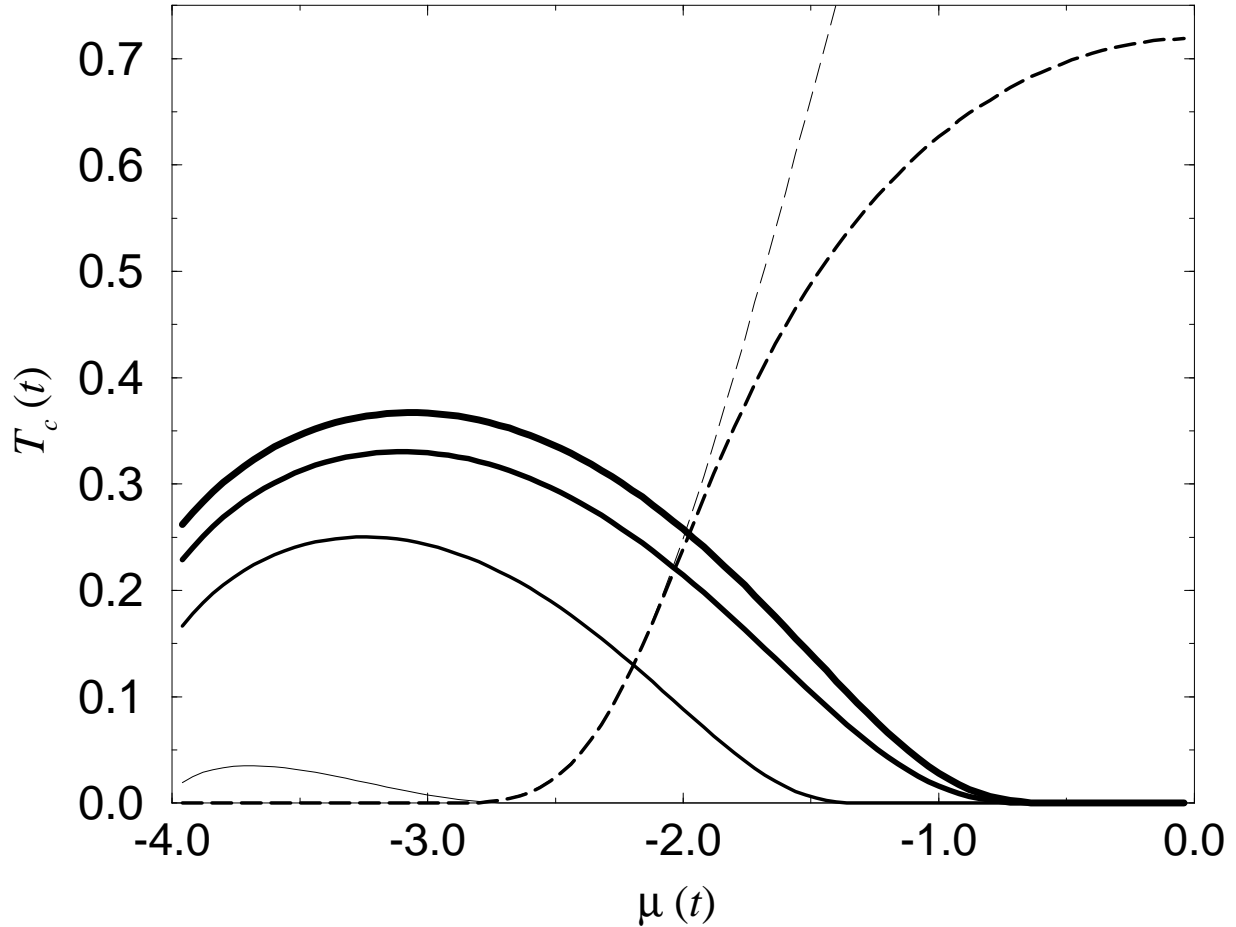


FIG. 3. The transition temperatures T_c are given as functions of chemical potential μ for $V_1 = 3t$. The solid lines correspond to the numerical evaluation of T_s for on-site repulsion $V_0 = 0, 2.5t, 3.5t$, and $\sim \infty$; linewidth decreases with increased V_0 . The d-wave transition temperature T_d (dashed lines) is unaffected by changes in V_0 . Note that the analytical (lighter dashed line) and numerical (darker dashed line) results for T_d still agree closely at low densities in this intermediate-coupling regime. The correspondence between the numerical and analytical results for T_s (not shown) continues for intermediate coupling but is found to improve with increased V_0 , or decreased T_s .

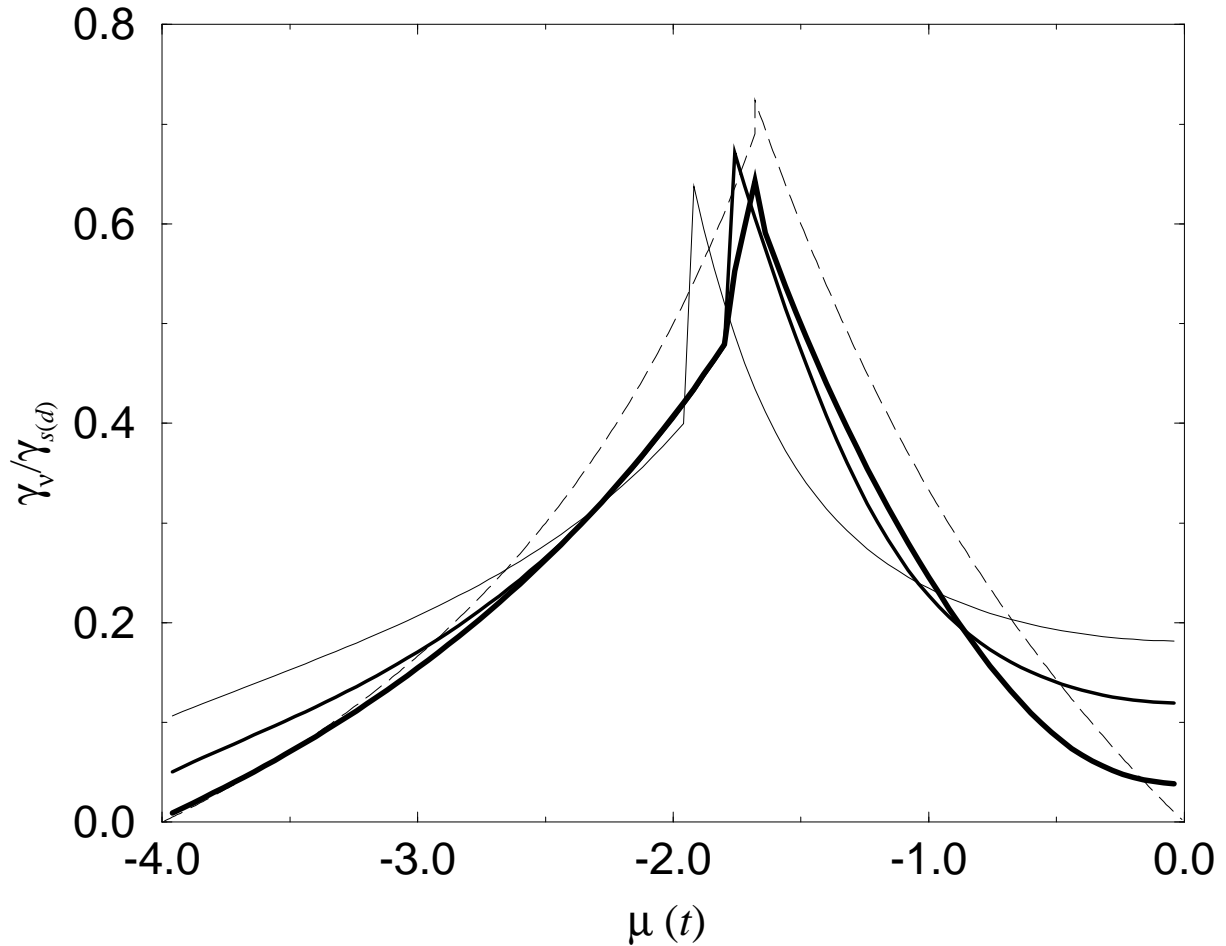


FIG. 4. The ratio of the mixed gradient coefficient γ_v to the ordinary gradient coefficient of the dominant order parameter γ_s or γ_d is given as a function of chemical potential μ . The solid and dashed lines correspond to numerical and analytical results respectively. The solid lines become progressively darker as V_1 is decreased from $3t$ to t in increments of t ; V_0 is taken to be zero. The discontinuity reflects the transition from an s-wave to d-wave bulk superconductor; the dashed line assumes that this occurs for $\mu = -1.65t$. All values are determined at the appropriate T_c .

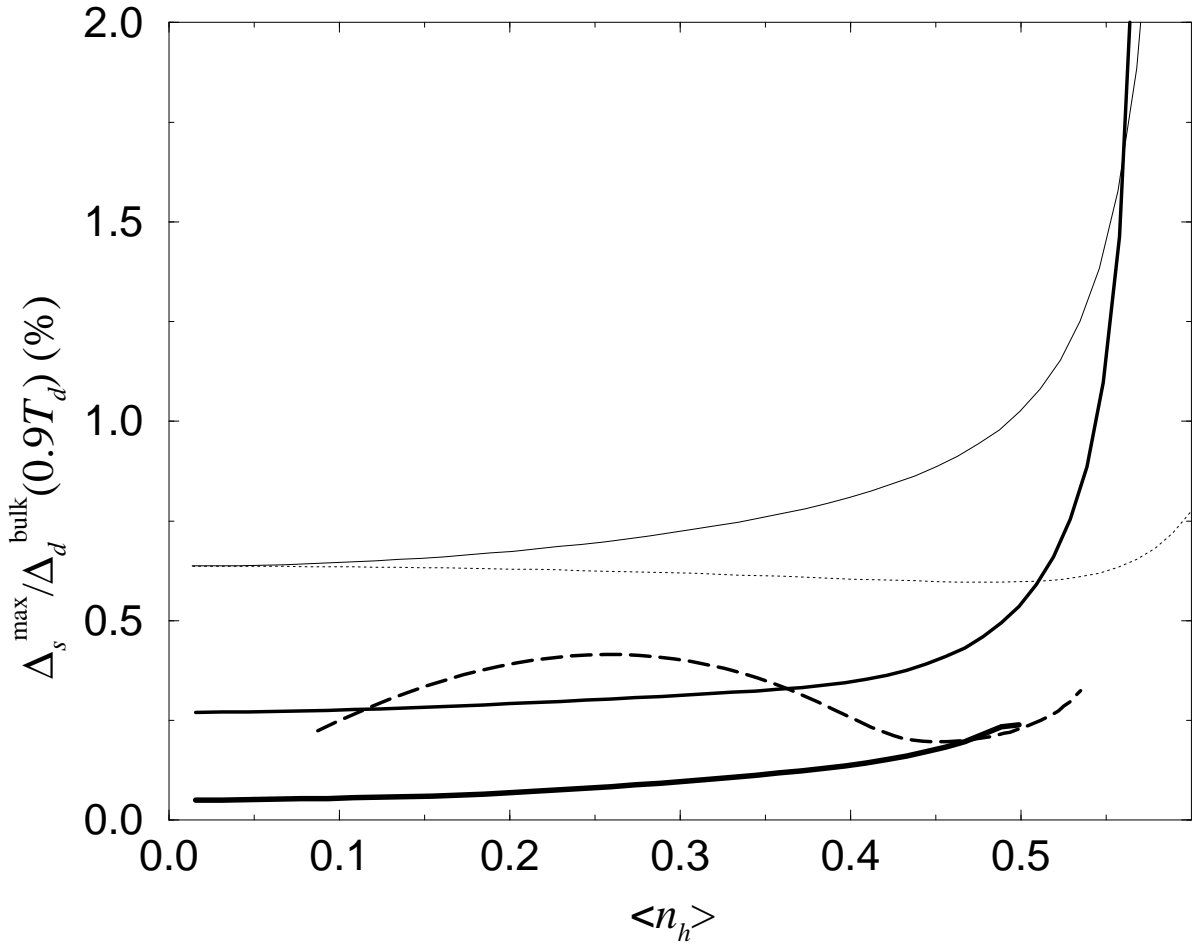


FIG. 5. The relative magnitude of the maximum s-wave component induced in the vortex core $s_{\text{max}}/d_{\text{bulk}}$ is calculated numerically and given as a function of hole density $\langle n_h \rangle$ for temperatures $T = 0.9T_d$. The dashed line, corresponding to results for the AvH model, indicates that the induced s-wave component is largest near optimal doping ($\langle n_h \rangle \sim 20\%$). Results for the EH model are given for comparison, where in the hole representation $\langle n_h \rangle = 0$ corresponds to $\mu = 0$; solid lines (in order of decreasing boldness) correspond to $V_1 = t, 2t, 3t$ with $V_0 = 0$, while the dotted line is for $V_1 = 3t, V_0 = 4t$.

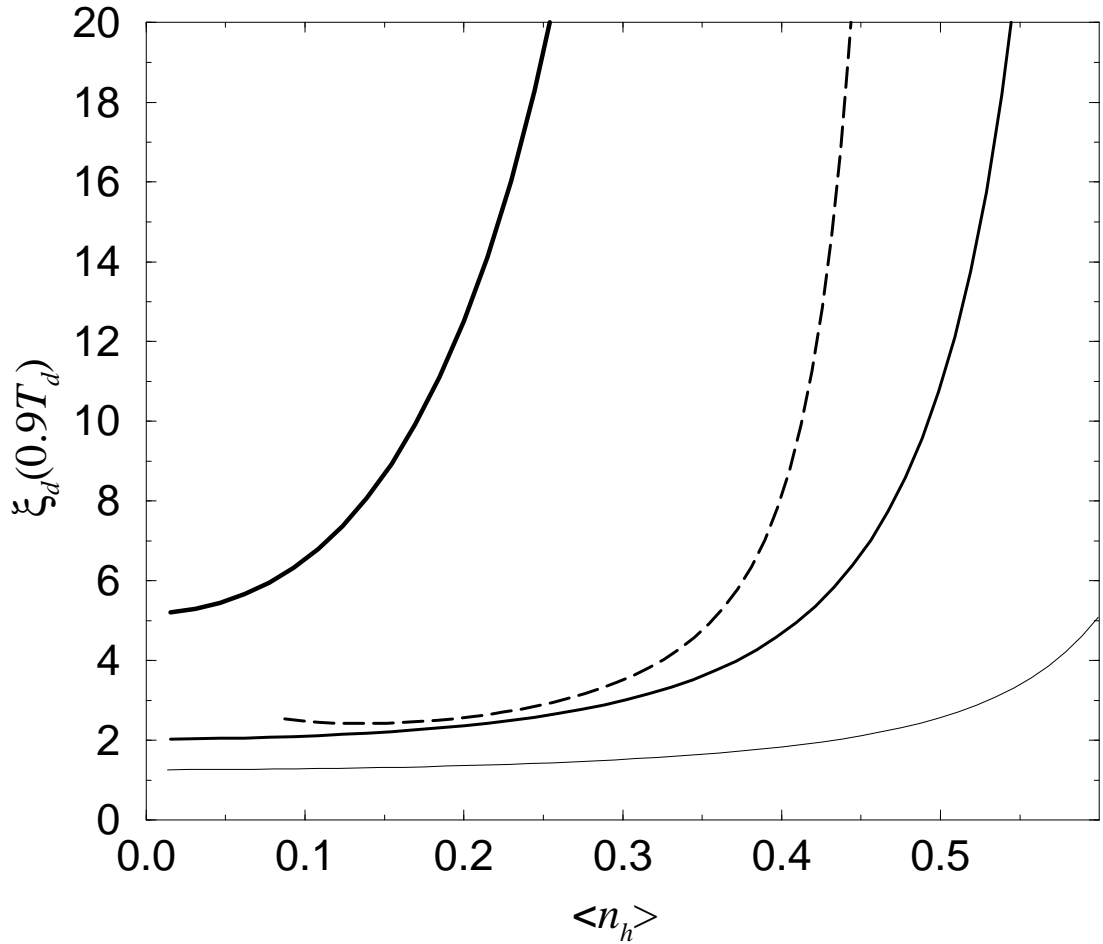


FIG. 6. The numerical d-wave Ginzburg-Landau coherence length $\xi_d(T)$, measured in units of a lattice spacing, is shown for $T = 0.9T_d$ as a function of hole concentration $\langle n_h \rangle$. The dashed line corresponds to the AvH model while the solid lines (in order of decreasing boldness) correspond to the EH model for $V_1 = t, 2t, 3t$ and $V_0 = 0$.

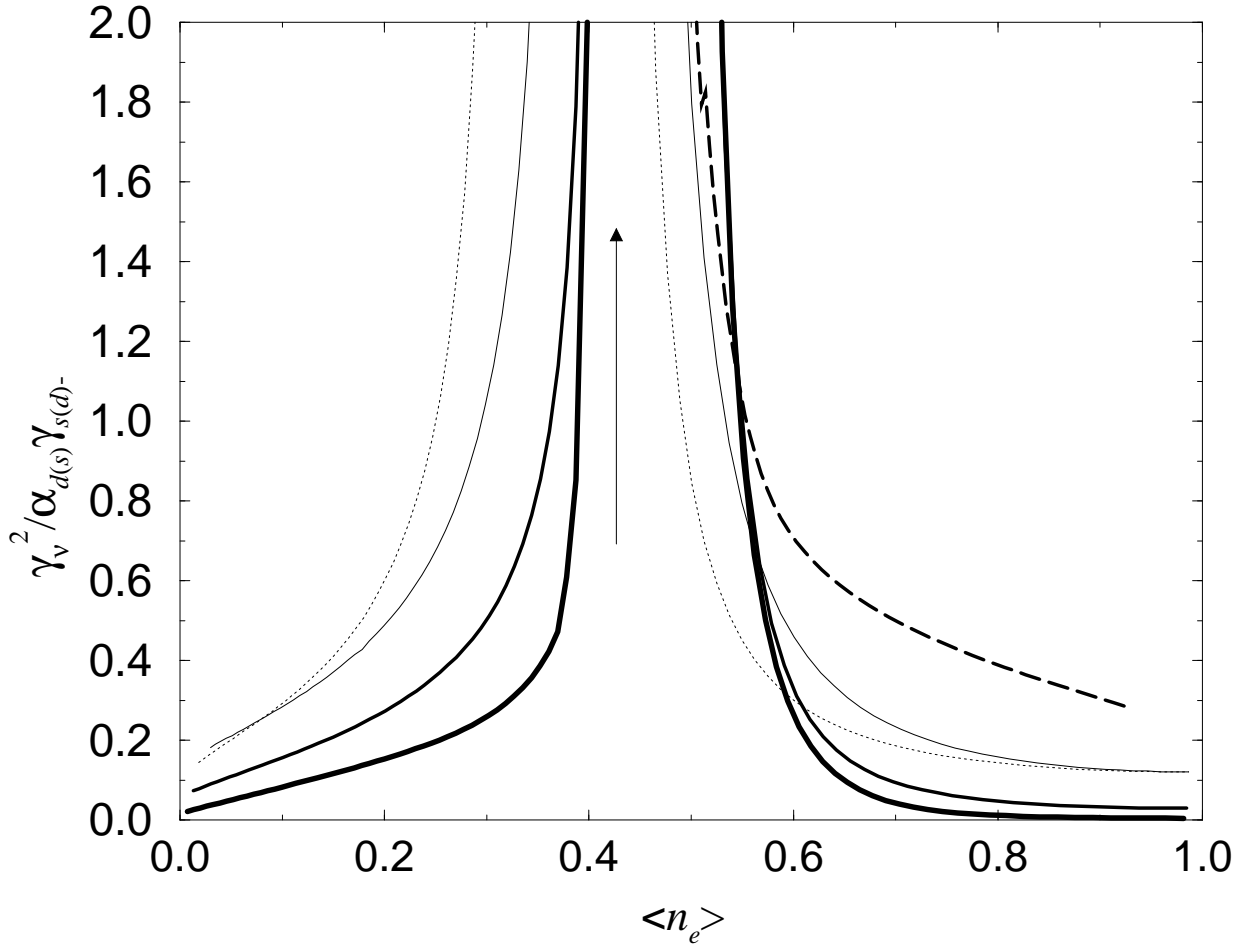


FIG. 7. The ratio $\gamma_\nu^2 / \alpha_{d(s)} \gamma_{s(d)-}$ is shown as a function of electron concentration $\langle n_e \rangle$ for $T = T_c$. Solid lines (in order of decreasing boldness) correspond to the EH model for $V_1 = 1.3t, 2t, 3t$ with $V_0 = 0$, while the dotted line is for the EH model with $V_1 = 3t, V_0 = 4t$. The dashed line gives the results for the AvH model in the electron notation such that $\langle n_e \rangle = 1 - \langle n_h \rangle$. To the left (right) of the arrow is shown $\gamma_\nu^2 / \alpha_d \gamma_{s-}$ ($\gamma_\nu^2 / \alpha_s \gamma_{d-}$) corresponding to bulk s-wave (d-wave) superconductivity.